Journal of Medical Robotics Research, Vol. 0, No. 0 (2026) 1–28
© World Scientific Publishing Company

Robotic Ultrasound-guided Percutaneous Interventions: A Review of Imaging, Perception, and Procedural Assistance

Hoorieh Mazdarani, Carlos Rossa

Department of Systems and Computer Engineering, Carleton University, Ottawa, ON, Canada.
E-mail: hooriehmazdarani@cmail.carleton.ca

Ultrasound-guided percutaneous interventions enable diagnosis and treatment through small incisions, offering reduced trauma, faster recovery, and broader patient eligibility compared to open surgery. Ultrasound offers real-time, radiation-free imaging with broad accessibility, yet outcomes and use of these procedures remain limited due to poor image quality, limited tool visibility, and demanding coordination between probe manipulation and instrument control. These challenges are tightly coupled system-level limitations propagating across the procedural workflow, ultimately affecting targeting accuracy and clinical adoption.
This paper offers a critical narrative review of representative methods addressing these challenges. Rather than cataloguing techniques by modality or algorithmic class, the review is structured along a progressive spectrum of assistance to the interventionist: (1) image-level assistance, spanning signal processing and learning-based reconstruction for artifact suppression and quality enhancement; (2) perceptual-level assistance, including segmentation, registration, compounding, and tool tracking to improve spatial understanding; and (3) interventional-level assistance, where robotic systems, augmented reality, and closed-loop feedback control translate improved perception into actionable guidance for probe stabilization and tool steering. By analyzing these approaches within a unified system-level framework, this review highlights current limitations and outlines research directions toward the next generation of robot-assisted and shared-autonomy ultrasound-guided interventions.

Keywords: Surgical Robotics; Ultrasound-guided Percutaneous Interventions; Minimally Invasive Robotic Procedures; Robotic Assistance; Robotic Ultrasound Imaging.

1. Introduction

In percutaneous interventions, internal organs or tissues are accessed through small punctures in the skin rather than larger open incisions. Using specialized needles, catheters, or probes, interventionists can diagnose and treat a wide range of conditions while minimizing trauma to surrounding tissue. Common examples include tissue biopsy [1, 2], tumour ablation in the liver and kidney [3–5], stone removal by percutaneous nephrolithotomy [6, 7], and catheter-based cardiac procedures [8]. These procedures offer substantial benefits compared to open surgery, including reduced bleeding, less postoperative pain, shorter hospital stays, and faster recovery times. It expands surgery eligibility to those who may not tolerate open surgery due to age, chronic disease, or other health conditions. These advantages have led to their widespread adoption across multiple medical fields, including urology, oncology, cardiology, and neurology [9, 10].

The effectiveness of these procedures largely depends on precise tool placement within a target. Fluoroscopy remains a well-established option for real-time guidance, but conventional systems provide only 2D projections with low soft-tissue contrast and require continuous radiation exposure. Modern C-arm systems can also reconstruct 3D volumes from rotational acquisitions, though not as a continuous stream during tool insertion. Computed tomography (CT) provides higher spatial resolution and better depth perception but involves higher radiation doses, higher cost, and longer setup time and is acquired intermittently rather than continuously. Magnetic resonance imaging (MRI) is a better choice when soft-tissue contrast is required, yet its operational complexity, cost, and the requirement for compatible tools limit its use [11, 12]. Ultrasound, in contrast, offers real-time, radiation-free imaging at a lower cost and has broad accessibility. It is one of the most commonly used imaging modalities in percutaneous interventions [13–15]. Ultrasound trades spatial resolution and soft-tissue contrast for continuous imaging, no ionizing radiation, low cost, and portability, and this combination makes it well suited for real-time tool guidance.

Ultrasound image quality is often degraded by artifacts

that arise from different sources. Speckle results from interference between echoes scattered within tissue and lowers the contrast between adjacent structures. Acoustic shadowing occurs when a strong reflector, such as bone, gas, or a metallic tool, blocks the beam and leaves the region beyond it without acoustic signal. Reverberation arises from repeated reflections between two strong interfaces, most often the tool shaft, and produces a series of false echoes below it. Image quality is further affected during the procedure by physiological motion, including respiratory cycles, tissue manipulation, variable probe pressure, and tool steering that displace and deform the target between frames. These limitations create substantial intraprocedural complexity. As a result, ultrasound is often paired with a complementary imaging modality, and the procedure usually becomes a three-step process.

In the first step, CT, MRI, or ultrasound is used preoperatively to scan the tissue, localize the target, and plan an optimal access path. The second step is intraoperative; the interventionist inserts a surgical tool to reach the target under ultrasound guidance. In this step, preoperative images are often registered onto real-time ultrasound images to estimate the location of targets and sensitive structures when they are poorly visible under ultrasound. Throughout tool insertion, the interventionist must continuously interpret ultrasound images to monitor tool position and adjust its trajectory in real-time to compensate for deviations and target motion. Image interpretation is highly operator-dependent, requiring significant skill to simultaneously coordinate the hand holding the ultrasound probe and the hand holding the tool. Image degradation caused by acoustic artifacts and partial target and tool visibility, combined with the need for precise probe/tool coordination, imposes significant challenges on procedural accuracy, particularly in deep or anatomically complex regions [3, 4, 16]. Tool visualization during insertion is also particularly challenging, as the angle of incidence between the ultrasound beam and the tool surface strongly affects the tool's appearance in the image; when the beam reaches the tool obliquely, specular reflection may direct most of the energy away from the probe, causing the tool to appear faint or invisible. The tools are often highly reflective acoustically, which blocks ultrasound waves and creates shadow zones that obstruct tissue visibility [17–19]. In the third and last step, once the tool is inserted in the tissue, the target is sampled or treated, and postoperative imaging verifies procedural success.

The challenges highlighted above also affect the interventionist directly. Sustained coordination between the ultrasound screen and the insertion site increases mental workload, particularly while locating the tool tip in the image [20]. Manual intervention is also subject to hand tremor, which adds to the displacement caused by respiratory motion and tissue deformation [21]. Prolonged scanning postures and continuous probe pressure also cause physical strain, and work-related musculoskeletal disorders are widely reported among ultrasound operators [22]. Together, these factors create a steep learning curve in ultrasound-guided percutaneous interventions, limiting their adoption by less experienced practitioners [19, 23, 24].

To address these limitations, leveraging advances in computer vision, artificial intelligence, augmented reality, and robotic assistance, substantial research has been devoted to enhancing image clarity, developing algorithms to automatically interpret the contents of an ultrasound image, and assisting the interventionist with both tool tracking and tool navigation. This paper presents a critical narrative review of the literature addressing the aforementioned limitations. Representative approaches are analyzed, synthesized, and organized into three principal categories based on the level of assistance provided to the interventionist in a progressive spectrum ranging from image processing algorithms to interventional robotic systems (see Fig. 1), as follows:

- **Assistance level 1** comprises image enhancement and artifact reduction algorithms to improve ultrasound image quality, including image filtering methods;
- **Assistance level 2** focuses on image enhancement for anatomical and tool visualization, including image segmentation and augmentation algorithms, unimodal and multimodal image registration, 3D imaging and image compounding, and methods to identify and track the tool in ultrasound images; and
- **Assistance level 3** leverages advancements from levels 1 and 2 in interventional assistance for tool navigation and ultrasound probe control, such as augmented reality, robotic assistance, and teleoperation approaches.

We selected representative works that introduce an underlying principle, illustrate adopted implementations, or report recent advances in the area. The review is therefore not exhaustive, and the omission of a work does not imply a judgement on its merit.

Unlike prior reviews that concentrate on isolated technical solutions, we analyze issues from a system-level perspective according to the degree of assistance they provide, structuring this survey along a continuum that follows the procedural workflow. Section 2 covers image enhancement and artifact reduction. Section 3 covers visual interpretability enhancement, from image segmentation and augmentation (Section 3.1) through multimodal and unimodal registration (Sections 3.2 and 3.3), image compounding (Section 3.4), and tool imaging and tracking (Section 3.5). Section 4 covers interventional assistance for tool and probe control, spanning tool insertion and steering (Section 4.1), ultrasound probe control (Section 4.2), and teleoperation and cooperative control (Section 4.3). Within each section, papers are grouped by the technical solution they propose. Finally, Section 5 discusses the reviewed solutions and outlines research directions. Section 5.1 summarizes the challenges and the role of each assistance level; Section 5.2 reviews the technical limitations that persist across all three levels; Section 5.3 examines the barriers to clinical translation; and Section 5.4 outlines future research directions and concludes the paper. Together, these approaches reflect

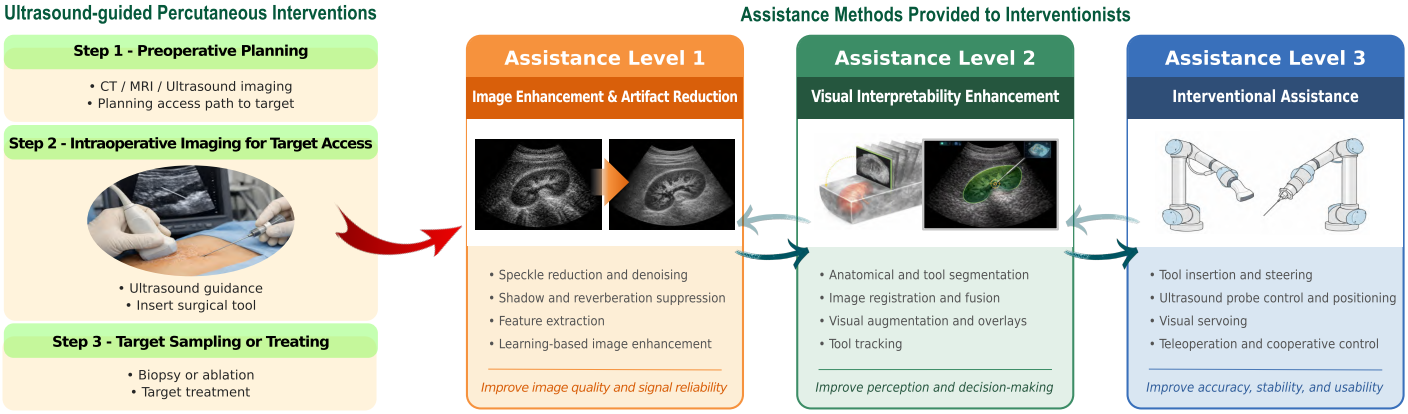


Fig. 1. Assistance methods provided to the interventionist during ultrasound-guided percutaneous interventions, divided into three principal categories based on the level of assistance in a progressive spectrum ranging from image processing algorithms to interventional robotic systems

current research efforts to mitigate the inherent limitations of ultrasound guidance and to support more reliable and accessible ultrasound-guided percutaneous interventions.

2. Assistance Level 1: Image Enhancement and Artifact Reduction

The limited resolution of ultrasound images and image artifacts such as reverberation and noise are major challenges in percutaneous interventions. The first level of assistance attempts to improve image quality with filtering for noise reduction and improved clarity.

Computer vision has been extensively applied to improve ultrasound image interpretation and procedural guidance. The initial step includes noise removal followed by image segmentation and feature extraction [19, 25].

Several studies have developed filters to reduce speckle noise in B-mode ultrasound images without losing diagnostic information. Such techniques range from classical computer vision methods, including spatial filtering, diffusion filtering, and wavelet filtering, to more recent approaches using deep learning [26–28]. Methods such as speckle reduction filtering, image segmentation, optical flow analysis, and multi-view compounding have been used to enhance spatial coherence and suppress artifacts [26, 29]. However, filtering speckle noise is challenging since noise cannot be uniformly modelled and is tissue-dependent [30–32]. Alternatives to deterministic filters include content-dependent smoothing approaches, like diffusion methods, which adjust the behaviour based on the local image features, thus preserving edges [33, 34]. Statistical methods can also be used for designing speckle-reducing filters [35], and variations that better preserve edge detection [36].

Other authors have used bilateral filtering [37, 38] or semi-adaptive thresholding with a diffusion function [39] to preserve details and improve noise reduction. Wavelet transform is also commonly used for noise suppression and feature extraction, and to determine which image features to eliminate while preserving the resolution of the original image [40]. In another work, a hybrid denoising method is proposed by considering the characteristics of the local speckle noise and the non-local mean filter [41]. In this study, speckle noise is modelled using local intensity distribution, while the non-local mean filter is applied to suppress additional noise by exploiting redundancy within the image. Wavelets are also employed by Tay *et al.* [42] to iteratively remove atypical data points and replace them with a local mean; however, wavelet filtering performance remains strongly dependent on the wavelet type, the ultrasound data, and the noise present in the image [43].

While the above filters can improve image quality, they lack robustness across patients and imaging settings, and real-time implementation can be computationally demanding [32]. Artificial intelligence and machine learning methods, such as support-vector machines, random forests, or k-nearest neighbours, have been shown to improve the ability to interpret complex ultrasound data and generalize across different populations [44]. Deep learning architectures have been applied to denoising, speckle suppression, tissue classification, needle detection, and anatomical segmentation [45]. These advancements marked a transition from analytical methods toward architectures that learn directly from raw ultrasound data.

Deep learning uses large datasets to learn image features directly from ultrasound data and automatically identify anatomical structures. Deep learning achieves near-real-time performance with high accuracy across multiple anatomical regions and imaging setups [46]. Several authors have used deep learning and convolutional neural networks for speckle noise reduction while preserving image details [45, 47, 48]. For example, ResNet-based denoising achieved a higher peak signal-to-noise ratio and structural similarity index when compared with classical median and Wiener filters, while still preserving edges [49].

While deep learning methods can substantially enhance image quality, training such networks requires clean,

noise-free images, which are often difficult to obtain. Unsupervised deep learning methods, such as the speckle-to-speckle approach [50], can alternatively be used for noise reduction without the need for clean reference images. These methods can achieve higher signal-to-noise and contrast-to-noise ratios than filtering while preserving anatomical information [50]. Deep learning has also been applied to reconstruct ultrasound signals from raw radio-frequency data. Neural network beamformers learn the mapping from raw channel data to B-mode images, reducing dependence on manual parameter tuning. Neural network-based and recurrent models can reconstruct high-quality images, enhance resolution, suppress speckle, and estimate tissue properties such as sound speed or attenuation [51].

More recent work has applied generative models to ultrasound image enhancement. Diffusion models learn the distribution of clean images and remove noise through iterative denoising, preserving tissue texture better than methods that assume additive noise. Such models have been used for denoising the images while ensuring the preservation of the speckle pattern [52] and suppressing the haze caused by multipath reflections [53]. Adversarial and hybrid formulations combine this process with feature extraction or generative adversarial networks for superior denoising and structural preservation performance [54,55]. Self-supervised methods can learn despeckling from a single noisy image without paired or clean data [56], which suits ultrasound imaging because clean reference images are rarely available. These methods report higher quantitative metrics and better structural preservation than filtering, but they introduce two concerns for interventional use. Generative models can produce structures that are not present in the original data, the iterative sampling process increases computation, which limits real-time use, and the effect of denoising on downstream tasks is not always uniform [57, 58].

Enhancement methods are subject to timing constraints and must be performed between image acquisition and image display without reducing the frame rate or introducing additional latency, which could potentially lead to tool placement errors. The computational cost varies across the methods discussed above, ranging from online local filters to diffusion-based methods, which are among the most demanding ones. Deep learning methods are now in the middle of this range, reaching near-real-time or real-time rates on dedicated hardware [46, 48]. However, comparison across methods is limited, since most works report image quality metrics such as peak signal-to-noise ratio, structural similarity, or contrast-to-noise ratio, without stating the processing time per frame.

3. Assistance Level 2: Visual Interpretability Enhancement

The next level of assistance attempts to improve the clarity and contextual understanding of ultrasound images, including segmentation, registration, image fusion, and visual augmentation of anatomical structures and surgical tools. The enhanced images provide an additional layer of assistance, helping the interventionist interpret ultrasound images, identify anatomical landmarks that are otherwise hard to see, locate tools within the images, and compensate for anatomical motion or deformation. Ultimately, this enhanced situational awareness benefits both expert and novice interventionists by reducing procedural workload for experienced clinicians [59] and shortening learning curves by simplifying tool guidance [60–63]. It can also improve targeting precision and reduce the risks associated with image misinterpretation. However, enhancing visibility in ultrasound images is challenging due to acoustic interference and image artifacts. The most commonly used methods are discussed in the next subsections (see Fig. 2).

3.1. *Image Segmentation and Augmentation Algorithms*

Ultrasound often provides only partial or distorted views of deep or obscured anatomical structures. Beyond image quality improvement, researchers have also developed techniques that can automatically identify (segment) and highlight important structures in the images (overlay/augment) (including bones, nerves, blood vessels, organs, and surgical instruments). The results of image segmentation are usually overlaid on top of the original ultrasound images as colour-coded masks, boundary contours, or other visual cues.

Applications of image segmentation and augmentation include automatic marking of anatomical structures to support nerve-block planning [46], detecting breast nodules [64–68], ovary tumours [69], kidney stones [70–78], localizing lung lesions [79] or liver lesions [80–82], and applications in needle steering in the prostate [83], and guiding anaesthesia delivery [84].

Segmentation algorithms are mainly divided into two categories: edge-based approaches, which detect abrupt changes in image intensity [85], and region-based approaches, which detect similarities of neighbouring areas quantifiable by predefined metrics [86]. Edge detection is a well-developed field within image processing and has served as the basis for many other segmentation techniques [87,88].

Examples of algorithms include statistical-based methods, such as Bayesian [89], modified Canny operator [90], region growing [91], and fast marching methods [92], and hybrid algorithms incorporating genetic algorithms [93,94], fuzzy logic [88, 95, 96], and neural networks [97–99]. They have been widely applied to improve edge-detection precision and robustness against noise and artifacts.

Deep learning has led to more robust segmentation algorithms [100,101]. For instance, Smistad *et al.* [59] applied a deep convolutional neural network to identify musculocutaneous landmarks in ultrasound scans. Wang *et al.* [102] used local-phase tensor and global-context tensor features to segment bone surfaces, providing intensity-invariant representations with good accuracy. U-net is also commonly

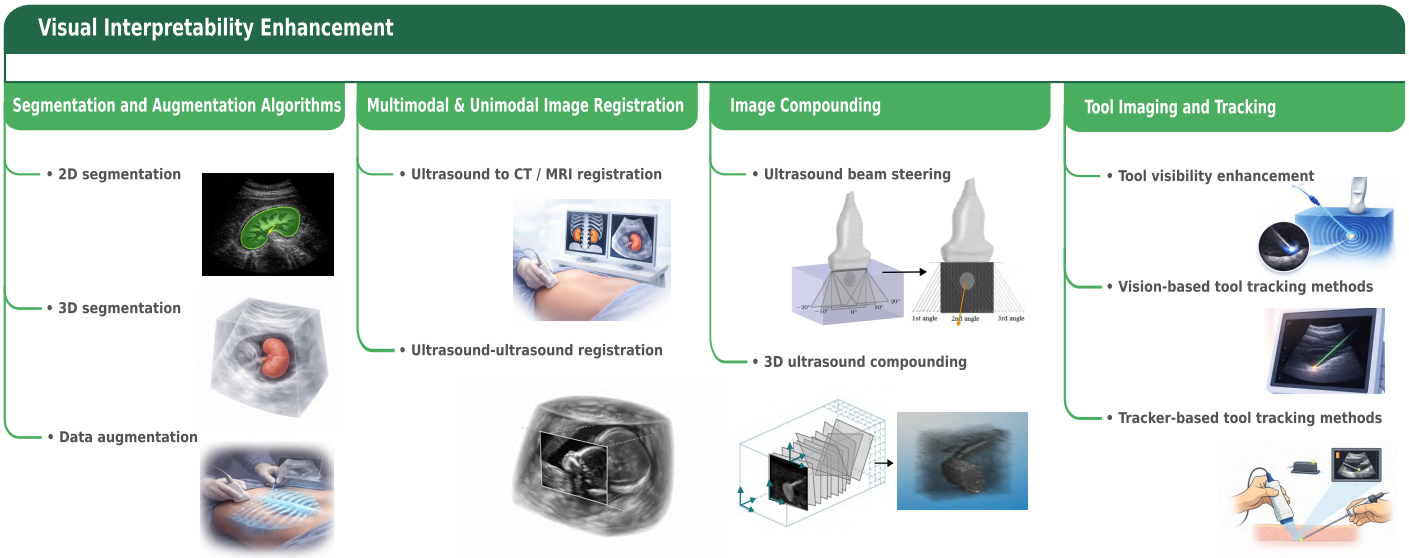


Fig. 2. Assistance methods to enhance visual interpretability of the intraoperative ultrasound images, including image segmentation, registration, augmentation, compounding, and tool tracking.

used in medical image segmentation. Almajalid *et al.* [103] and Chen *et al.* [104] proposed one of the first applications of U-net to segment breast ultrasound images. Khouy *et al.* [100] introduced GA-UNet; an extension of U-net that employs genetic algorithms to automatically design U-shape convolutional neural networks with reduced complexity. Cai *et al.* [69] proposed a hybrid architecture based on transformer and U-Net with a joint loss function. Transformer-based models capture long-range dependencies that convolutional architectures cannot, thereby combining a U-Net encoder-decoder with parallel transformer attention to model both local and global features. This approach showed superior performance compared to the segmentation methods based on neural networks when applied to the branchial plexus network and fetal head image datasets.

While such methods address different challenges in tissue segmentation, they often require expert knowledge, involve several tuning parameters, and demand substantial computational resources [100]. To address this limitation, Qian *et al.* [105] proposed a novel approach based on neural networks and multi-scale dilated convolution, demonstrating enhanced performance on breast ultrasound datasets.

Building on 2D methods, 3D segmentation has also been used to detect anatomical structures in ultrasound images. Marsousi *et al.* [106] proposed a 3D segmentation algorithm to detect the kidney shape and segment it in an ultrasound volume. They used offline training with prior knowledge of the kidney model, integrating it with anatomical information from the ultrasound data. Another study introduced automatic recurrent neural networks to segment multiple anatomical structures from prenatal volumetric ultrasound, including the fetus, gestational sac, and placenta [107]. Similar approaches are also employed by Xu *et al.* [64] for segmenting 3D breast ultrasound images, including fibroglandular tissue, fatty tissue, mass, and skin.

Segmentation foundation models are trained on large and diverse datasets and produce a segmentation from a prompt, such as a point or a bounding box, rather than being trained for one anatomical target [108]; however, their accuracy drops when applied directly to ultrasound images because of low contrast, unclear boundaries, and speckle [109]. Several works therefore adapt them to ultrasound. [110] adapts the Segment Anything model (SAM) for ultrasound image segmentation. It adds a convolutional branch to the image encoder and reduces the input size, which lowers the computational cost and improves performance on ultrasound datasets, and replaces the manual prompt with an automatic prompt generator so that segmentation runs end-to-end. Other works train these models on combined open-access ultrasound datasets to cover multiple anatomical sites [111, 112], or add task prompts and anatomical priors for multi-organ segmentation [113]. Extensions to video allow a target to be segmented across consecutive frames from a single prompt, which is relevant to real-time guidance [114]. Text prompts have also been used to select the target organ [115]. These models reduce the need for task-specific training data and generalize better across imaging settings than networks trained on a single dataset. Their main limitations are the computational cost of large encoders, the dependence of accuracy on prompt quality, and the small proportion of ultrasound data in the datasets used for pretraining.

While 2D and 3D segmentation can be used to identify important image landmarks, certain lesions and anatomical structures may not be visible under ultrasound, especially if they are obscured by bone or air [116]. Another critical issue is target motion, caused by respiratory cycles, tissue manipulation, variable ultrasound probe pressure, or tool steer-

ing, which can lead to tissue deformation and spatial misalignment of segmented images and targets [117]. Furthermore, highly reflective structures, such as bones, air pockets, and surgical tools, often create acoustic shadow zones that obscure anatomical structures in the images [18, 19]. Metallic tools tend to appear distorted under ultrasound due to reflections. This issue becomes more pronounced in interventions involving multiple probes, such as liver ablation, where overlapping shadows and reverberations often obstruct the target area, increasing the risk of tool misplacement. In such cases, multimodal image registration is necessary.

Other than image overlay, segmented information can be conveyed using augmented reality to enhance the operator's spatial perception and situational awareness [60–62, 65,70,88,118]. Augmented reality overlays 3D anatomical or tool information directly onto the patient or the ultrasound display, creating an intuitive correspondence between imaging data and physical anatomy [61, 63, 84, 118–122]. Such systems typically use complementary tracking devices, such as electromagnetic, optical, or mechanical trackers, to provide precise localization of both the ultrasound probe and interventional tools in 3D space [61,123]. These systems enable image-to-world registration, facilitate real-time navigation, and support multimodal image fusion, allowing the operator to plan and execute interventions with greater accuracy and confidence.

A trainee learning ultrasound guidance must build a mental map between 2D images and the anatomy beneath the probe. Augmented reality makes this correspondence explicit rather than leaving it to be inferred. A study of ultrasound-guided catheterization found that trainees using a head-mounted augmented reality overlay completed critical steps faster and reported lower mental workload than when using the ultrasound display alone [20]. Used in training, these systems allow the image-to-anatomy correspondence to be learned before the trainee works under the pressure of a clinical procedure and may shorten the learning curve.

3.2. *Multimodal Image Registration*

When the target is not visible or is poorly visible under ultrasound, information from preoperative images (such as CT or MRI) can be fused with intraoperative ultrasound. While interventionists have traditionally performed registration manually during the procedure, recent advancements in computer vision have both improved accuracy and functionality. These methods involve the use of various transformation models, similarity measures, and optimization techniques to better locate the corresponding areas across imaging modalities [116, 124].

Traditional metric-based and feature-based registration methods commonly rely on iterative optimization, statistical approaches, and custom features. Some classical methods include mutual-information-based [125, 126], entropy-based [127, 128], wavelet-based [129], and contour-based [130, 131]. For instance, Keil *et al.* [132] registered vessel structures visible in contrast-enhanced CT with B-mode ultrasound, improving target registration accuracy. In another work [133], a voxel-based algorithm performed non-rigid registration between 3D ultrasound and CT by combining intensity and gradient information, with a mean alignment error under 2 mm and lesion registration error under 3 mm. Another similarity-based algorithm is provided in [134] for ultrasound-CT image registration. In [135], an automated ultrasound-CT registration method is presented to align the posterior vertebral surface extracted from CT with that seen in ultrasound to assist with image-guided spine surgery. In this method, forward and backward scan-line tracing produce point clouds, which are registered on intraoperative ultrasound scans.

MRI-ultrasound image registration has many practical applications. Gong *et al.* presented a non-rigid MRI-transrectal ultrasound image registration algorithm that uses correlation ratio-based mutual information as the similarity criterion [136]. In [137], the authors presented an automated registration method to fuse preoperative MRI scans of the prostate with real-time transrectal ultrasound images during prostate cancer biopsy. The method delineates the prostate on MRI, constructs a probabilistic model of prostate location in transrectal ultrasound images, and aligns the MRI-segmented prostate with this probabilistic model. Another study used a random forest and Hough transform for automatic prostate segmentation on transrectal ultrasound, combined with coherent point drift and thin-plate splines for deformable registration [138]. The system successfully mapped suspicious regions observed in positron emission tomography or MRI scans onto interventional transrectal ultrasound images. Non-rigid registration between these imaging modalities has also been addressed in [136] using correlation ratio-based mutual information as the similarity metric.

To address intraoperative target motion, Weon *et al.* [139] proposed a real-time system that registers 2D ultrasound images to a 4D preoperative volume reconstructed from CT or MRI data. While the patient was breathing, a fixed 3D ultrasound transducer established initial rigid registration, and candidate slices were matched using gradient-based similarity, accounting for respiratory-induced image deformation. In another study [140], a rigid deep learning method registered preoperative CT to sparse freehand ultrasound by maximizing a similarity correlation ratio.

More recent studies have shifted focus toward surface-based registration. Gomes *et al.* [141] extracted contours from 3D ultrasound and CT images of a porcine kidney. Then, they misaligned CT surfaces to simulate positional variability and registered the images using iterative closest point regression. Another work performed an initial cranio-caudal ultrasound sweep and roughly aligned CT and ultrasound, followed by gradient-based alignment of the posterior surface [142], improving speed and accuracy. In [143], a custom CT-to-3D-ultrasound algorithm registers a preoperative vertebral model to the vertebral surface, reconstructed through 3D ultrasound. The algorithm

includes a pre-alignment phase using symmetry information, followed by iterative closest-point registration using a Gaussian pyramid intensity model.

Like in image segmentation, image registration methods often require manual tuning of several parameters, which can lead to slow convergence and poor registration performance [144]. Deep learning provides a data-driven alternative, reducing some of these limitations [145]. For instance, a similarity-metric-based method using a regression neural network was proposed by Haskins *et al.* [146] to register MRI and transrectal ultrasound images, which showed better performance than mutual information-based approaches. Another method uses foundation models in [147] to minimize model training requirements. Experimental results on MRI/ultrasound registration demonstrated better performance over learning-based methods.

Other works use vision foundation models as feature encoders rather than as segmentation models. Features learned from large image datasets are similar across modalities, which helps align images whose intensities differ [148]. This idea has been extended to registration models that accept a target deformation or constraint as an input, and to frameworks that transfer cross-modal features from a pretrained encoder to the registration network [149, 150]. These methods reduce the amount of paired training data required, which is the main practical limit in ultrasound registration, since paired preoperative and intraoperative data are difficult to obtain. Surface-based registration remains an alternative when intensity-based alignment is unreliable. A recent example registers a preoperative model to a point cloud of the bone surface extracted from ultrasound for robotic spine surgery [151].

3.3. *Unimodal Registration (ultrasound-ultrasound)*

Besides multimodal image registration, unimodal ultrasound-to-ultrasound registration can also be used to improve spatial perception [152]. Typically, these algorithms involve acquiring a preoperative ultrasound volume to capture the full anatomy of the target region, and then registering real-time 2D ultrasound images onto this reference volume. Such frame-to-volume registration is particularly useful in prostate cancer biopsy, where 2D frames acquired with a transrectal ultrasound probe are aligned to a preoperative 3D ultrasound volume [144]. This helps the interventionist accurately position the biopsy needle in a suspicious lesion that may be poorly visible in individual 2D slices but more easily segmented from a 3D volume. The framework in [144] consists of three major components: a frame-to-frame registration network that estimates the current frame's 3D spatial pose, a frame-to-slice correction network that refines this estimate using information from the 3D ultrasound volume, and a similarity-based filtering mechanism that selects the slice with the highest correspondence to the incoming frame. Brooks *et al.* [153] explored a similar concept and used image correlation to directly register 2D ultrasound slices to preoperative volumetric data.

3.4. *2D/3D Ultrasound Image Compounding*

Another form of unimodal registration is ultrasound image compounding [25, 154]. Typically used to circumvent obscured areas in 2D images and recover important structures that are obscured by shadows, air pockets, or highly reflective objects, image compounding selectively combines information from multiple ultrasound slices acquired from different directions to form a single 2D image. The two main types of image compounding are 2D compounding from beam steering, and 3D spatial compounding, the latter combining slices from tracked sweeps of the target area [155, 156].

In 2D compounding, ultrasound images are acquired from multiple angles by steering the ultrasonic beam electronically without physically moving the transducer. The images captured from these different directions are then merged into a single compound image [157]. By selectively discarding information from shadowed regions, this approach can partially reduce shadows created by tools and bones. However, 2D beam steering is limited to a small sweeping angle, typically between $-10°$ to $10°$, and therefore, it may not completely eliminate shadowing artifacts [156, 158, 159].

In 3D spatial compounding, multiple 2D images are acquired by physically angling the ultrasound probe to capture images from different perspectives [158–160]. The individual images are then analyzed and combined to fill in shadowed areas with valid data. To combine these images, [161] developed a method that assigns regional weights to pixels depending on the local incidence angle of the ultrasound beam. Another method uses multiscale information to weigh the contributions of each image in the final compounded image [162]. In [163], image features are used to remove outlier pixel intensities due to artifacts and to downweigh inconsistent regions. Once the volumetric image is formed, it can be sliced along any desired imaging plane to generate new 2D images with greater detail than an equivalent single 2D image acquired from the same angle.

While traditional 3D compounding methods improve shadow removal and image quality compared to 2D beam steering [156], they cannot distinguish regular image data from shadows, often resulting in missing or distorted anatomical structures. In particular, they tend to retain high-intensity pixels, which may arise from unwanted reverberations in the image. To minimize this problem, probabilistic methods capable of distinguishing regular data from shadows may be considered to weigh the contribution of individual images in the final compounded image. In [164], a support vector machine generates probabilistic maps to detect shadows in each image before combining them. An evolution of this method, presented in [165], uses a convolutional neural network to estimate the images' echogenicity

and weigh each slice accordingly. To reduce dependency on large labelled datasets required for training, multi-scale image fusion using Laplacian pyramids can be tuned to retain only the most prominent image features and reject outlier pixels [166]. To deal with uncertainties in attenuated regions, [167] used confidence values as a weighting parameter to compose several image clusters. Confidence values, together with pixel intensity, are then used in [168] to remove needle-induced shadows and reverberations, while highly informative regions are compounded to create an accurate volumetric representation.

Most of these algorithms rely on devices that track the position of each frame with respect to a reference volume [169], such as optical trackers [156, 170–173], electromagnetic sensors [174–178], inertial measurement units [179–181], and others [154,182]. For instance, [174] used an electromagnetic tracker connected to the probe to record its 3D position with respect to the tracker base unit. In [170], an optical tracking device is used instead to capture the probe position. All these approaches require initial calibration [154], adding complexity to the procedure, while still being subjected to error, especially for lower-accuracy electromagnetic and optical trackers. Furthermore, tracking methods only record the position and orientation of the ultrasound probe and do not account for tissue deformation or movement. Therefore, feature-based image registration is still required to refine the tracker's initial registration estimate [25].

These limitations have motivated the development of trackerless approaches, such as neural network-based reconstruction methods that integrate inertial measurement data [179,209]. In this framework, 2D ultrasound images are acquired with a handheld probe, and optical flow combined with probe orientation data is used to estimate both local inter-frame and global transformations. Although such methods are generally less precise than tracker-based methods, they provide an effective alternative to additional sensors [144, 155].

3.5. *Tool Imaging and Tracking*

Targeting accuracy in percutaneous interventions depends heavily on real-time feedback of the position and orientation of the tool relative to the target. In ultrasound images, surgical tools like needles and catheters are slender, produce specular reflections in ultrasound images, and often appear intermittently in the images because their visibility depends on the insonation angle [186, 210, 211]. A wide range of methods have been proposed to improve tool tracking in ultrasound images, including computer vision algorithms [61, 185, 187, 191], custom needles visible under Doppler [212], and electromagnetic or optical trackers [203–205, 208, 213, 214].

Machine learning-based algorithms that learn from large annotated datasets have also been proposed. A deep learning method for directly extracting the 3D needle-tip position from sparsely sampled ultrasound volumes is presented in [190]. Yan *et al.* combined a motion-prediction transformer, a visual tracking model, and a data-fusion module to track the needle tip in a sequence of ultrasound images [191]. Zhang *et al.* introduced a framework that integrates a hybrid encoder combining a convolutional neural network and a transformer, along with an optical-flow estimation method for real-time needle segmentation and tracking [192]. Vision transformers have also been applied to detect the needle in ultrasound images [193]. Their results indicate that deep learning models are more robust to speckle and variable needle orientation than deterministic algorithms. Recent work has reduced annotation requirements of these methods. Self-supervised approaches learn tool motion from image sequences without manual labels [194], and other methods use an external signal, such as an induced vibration, to generate training targets automatically [195]. Segmentation foundation models have also improved generalization across ultrasound datasets, as discussed in Section 3.1; however, their benefit for tool tracking is less established, as tools are thin and of low contrast, their appearance changes with the insertion angle, and they are underrepresented in the datasets used for pretraining. Alternatively, volumetric ultrasound images provide more detailed information about the position of the tool than 2D images and can often detect curved tools in the images without assuming a straight shape [188–190, 215–217].

To track a needle in longitudinal ultrasound images, a common approach is to model the needle shaft as a straight line using the Hough transform [183,184]. With a sequence of sagittal images, a Kalman filter is often used to predict the location of the shaft in each slice [187]. Others employed optical flow to estimate frame-to-frame motion patterns that correspond to the tool's displacement within the ultrasound image [185]. Custom needles with embedded vibrating actuators at the tip [196,197] or at the base [198], have also been proposed to generate detectable Doppler signatures, at the cost of lower frame rate and image detail [84,212]. Another approach is to pass an optical fibre along the needle shaft to emit a laser beam at the tip, creating a localized acoustic response that enhances tip detection with a standard ultrasound transducer [199–202]. More recently, Cheng *et al.* used a needle equipped with an embedded optical fibre to capture optical signals along the shaft and combined these signals with ultrasound images and convolutional neural networks to improve tracking accuracy [218].

Electromagnetic tracking systems use sensors mounted on the needle and the ultrasound probe that respond to an external magnetic field. The measured tool position is registered relative to the probe and overlaid on the ultrasound images [203–205, 213, 214]. These systems require a larger trocar for sensor integration; the need for additional equipment may disrupt the workflow, and the presence of metallic objects can deteriorate measurement accuracy [84, 123, 205]. Other researchers have developed alternative tracking methods with other types of sensors attached to the needle, but these also come at the cost of added complexity [199, 201, 202, 206–208, 218–221].

Table 1. Tool segmentation and tracking methods in ultrasound-guided percutaneous interventions

Method	Principle	Advantages	Limitations
Computer vision	Hough transform to detect tool [183, 184]; optical flow tracking [185]; Kalman filter to predict motion [186, 187].	Non-invasive; no extra sensors; works with 2D ultrasound images.	Prone to noise and artifacts; cannot account for out-of-plane motion.
Tracking in 3D images	Volumetric ultrasound imaging [188–190].	Captures curved trajectories; improves spatial understanding.	Computationally intensive; needs volumetric data; low frame rate.
Learning-based methods	Neural networks for segmentation/tracking [190–192]; transformers for motion prediction[192]; vision transformers for tool detection [193]; self-supervised and few-shot learning to reduce annotation requirements [194, 195].	Robust to speckle noise; handle complex motion; enable real-time decision; self-supervised methods reduce the need for annotated data.	Performance still depends on training data coverage; generalization to thin, low-contrast tools remains limited; requires GPU hardware.
Visibility enhancement	Induced vibrations for Doppler enhancement [196–198]; needles with optical-fiber [199–202].	Enhanced visibility; Feedback improves localization.	Modified needles; reduced frame rate (Doppler); procedural complexity.
Electromagnetic tracking	3D position sensors attached to the needle [123, 203–205].	Real-time tracking; out-of-plane localization.	Distortion near metal; external hardware; procedural complexity.
Optical tracking	Stereo cameras or optical sensors track position [206–208].	spatial accuracy; suitable for navigation and registration.	Needs line-of-sight; cannot capture bending; procedural complexity.

Optical trackers are also commonly used to estimate probe and needle poses with comparable accuracy to that of an electromagnetic system [207, 208, 212]. Optical trackers can only measure the position of the base of the tool, from which the tip position is estimated, assuming the tool is rigid [206]. However, if a bevelled needle or a flexible tool is used, the tool tip follows a curved trajectory during insertion [210]. In such cases, a needle-tissue interaction model is often combined with the tracker to estimate needle tip position based on the location of its base [222–227]. Another major limitation of optical trackers is that they need a direct line of sight, which limits their application in certain procedures [84].

Table 1 summarizes the main strategies proposed to enhance tool visualization in ultrasound images along with their advantages and limitations.

4. Assistance Level 3: Interventional Assistance for Tool and Probe Control

Arguably, the main challenge in percutaneous interventions is the procedural complexity. Ultrasound-guided percutaneous procedures demand a high level of dexterity and coordination from the operator, as they must simultaneously manipulate the ultrasound probe with one hand while inserting and steering the needle or tool with the other. Orienting and stabilizing the ultrasound probe to maintain a clear view of the target is particularly challenging when the target is deep or mobile. The required proficiency in interpreting ultrasound images, aligning tools with imaging planes, and compensating for artifacts creates a steep learning curve and requires extensive training. Inexperienced operators often tend to prolong the procedure and achieve lower accuracy than experienced operators [24].

While image enhancement, segmentation, and augmentation can improve tissue and tool visibility, interventional methods such as robotic assistance can significantly alleviate the cognitive workload and enhance procedural outcomes. Robotic assistance in ultrasound-guided percutaneous interventions has been the focus of significant research and interest over the last two decades [228, 229]. Robots can be used to: (a) automate or semi-automate needle/tool placement along planned trajectories [62, 230], (b) stabilize and actively control the orientation, pose, and contact force of ultrasound probes to maintain consistent image quality [231], and (c) enable cooperative control to combine clinical judgment and robotic precision [60] (see Fig. 3).

4.1. *Assistance with Tool Insertion and Steering*

A wide range of methods has been proposed to assist surgeons in inserting the surgical tool along a planned

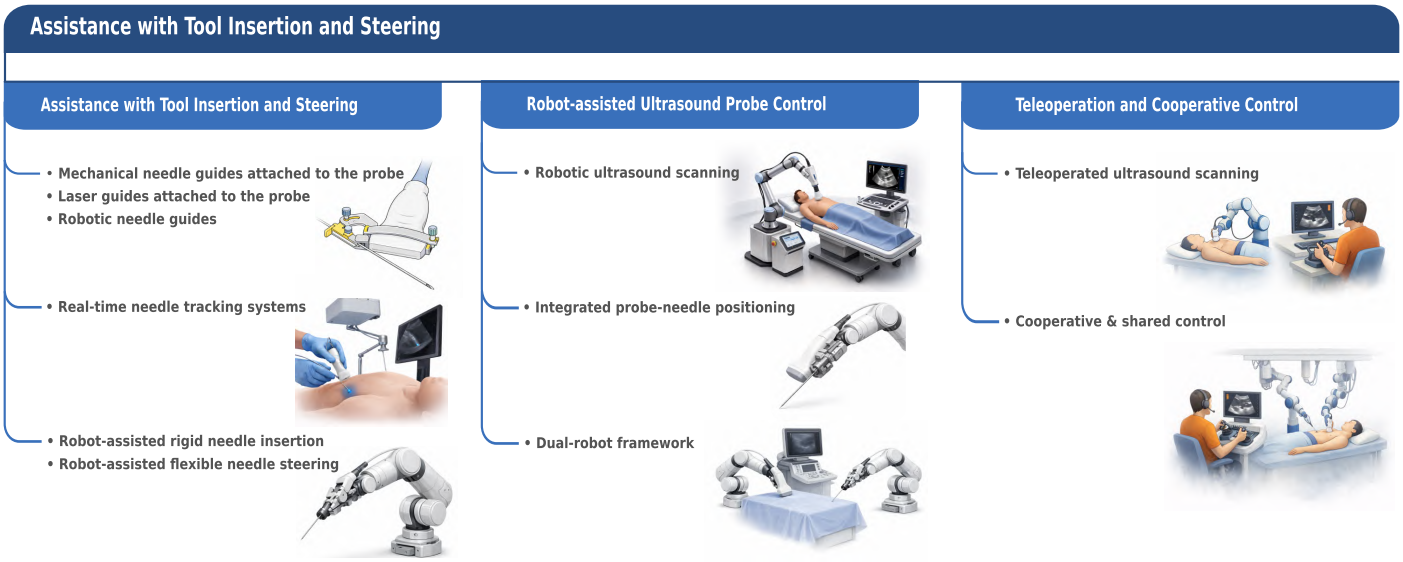


Fig. 3. Assistance methods provided for tool and probe positioning, including assistance with tool insertion, assistance with probe positioning, and teleoperation.

Table 2. Summary of assistance methods in order of complexity for tool insertion in ultrasound-guided interventions

Method	Principle	Advantages	Limitations
Needle guides	Guide attached to ultrasound probe aligns tool with imaging plane [84, 232–235].	In-plane alignment; better tool visibility; short insertion time for novices.	Limited flexibility; out-of-plane deflection; minimal benefit for experts.
Laser guides	Laser attached to the probe displays best insertion line on the skin surface [84].	Simple, low-cost visual cue; no mechanical constraint.	Prone to out-of-plane deviation; limited accuracy after insertion.
Tracking	Sensors or cameras track the pose of the needle and probe [203–205, 208].	Real-time guidance; compensates for hand tremor; overlay on ultrasound image.	Requires hardware and calibration; sensitive to interference/occlusion.
Tool guidance	Robot orients needle guide relative to probe [236–238].	Precise insertion angle/depth; reproducible trajectories.	Complex; calibration affects accuracy; reduced force feedback.
Rigid tool insertion	Tool on robotic arm; ultrasound or optical tracking guides insertion [239–242].	Autonomous or semi-autonomous insertion; image feedback for closed-loop control.	Large footprint; reduced ergonomics; needs real-time tracking.
Flexible tool steering	Robot controls steering manoeuvres (rotation, bending) [16, 243–245].	Compensates for tissue/tool deformation, better targeting with fewer insertions.	Complex actuation and control; may require custom tools.

trajectory while keeping it within the ultrasound imaging plane. These methods include 3D ultrasound and augmented reality, custom steerable needles [212], mechanical guides [232–235], electromagnetic, optical, or surgical navigation/tracking systems [203–205,208,213,214], and robotic assistance [236, 237, 244].

The simplest form of assistance is a mechanical guide attached to the ultrasound probe through which the tool is passed to align longitudinally with the imaging plane [84, 246]. At the cost of limited flexibility, a tool guide can improve tool visibility and reduce procedural time; benefits that are mostly reported by inexperienced practitioners. However, tool guides have not been shown to improve patient satisfaction or success rate [84]. For example, needle guides are commonly used with transrectal ultrasound probes in prostate biopsy [232]. Similarly, multi-angle needle guides can help reduce the completion time and enhance needle visualization for novice sonographers but with

no significant reduction in the number of needle insertions or improvement in targeting accuracy [233]. Needle guides used for ultrasound-guided central venous catheterization in [235] shortened the insertion time and improved the procedure's success rate. Instead of a mechanical guide, which keeps the needle insertion point fixed with respect to the probe, a laser guide has been proposed to project the optimal insertion path on the surface of the tissue [84]. However, laser guides do not guarantee that the needle stays in the imaging plane after insertion.

To restore some flexibility, researchers have also developed actuated mechanisms that automatically position the needle guide relative to the imaging plane [236–238]. For example, the 2-DOF system in [236] orients the needle guide while leaving the operator in charge of insertion but imposes a fixed maximum insertion depth. In other studies, robots were designed to improve precision during needle puncture, and to plan an insertion path based on the location of the target [232, 237, 238]. Offering an additional level of dexterity and flexibility, multi-DOF robotic needle insertion systems aim to alleviate the surgeon's cognitive workload, compensate for needle deflection, enable active needle steering, and reduce the number of insertions [16, 61, 210, 247].

Robotic assistance has been proposed for percutaneously steering needles and nephroscopes in a wide range of ultrasound-guided interventions, including kidney access [240], prostate brachytherapy [83, 244, 245], and tumour biopsy and ablation [16, 242, 248, 249]. For example, Adebar *et al.* [243] developed a needle steering robot combined with a new imaging approach in which high-frequency vibration of the needle makes it visible in ultrasound Doppler images. Later, a similar hand-held needle steering assistant device was proposed in [244]. It calculates control actions based on the needle-tissue interaction model and rotates the needle while the surgeon is inserting it, aiming to follow a straight line. A similar approach is used in [245] for steering a bevelled-tip needle by adjusting the needle orientation to reduce the tissue trauma. Other approaches use similar systems to steer a needle along a predefined, often curved trajectory [21, 239–242]. In [239, 241], the needle is attached to a robot arm and controlled via 2D ultrasound imaging to reach a target. A similar configuration is used in [242], where a biopsy robot is controlled via an optical tracker to sample the liver. Steering a flexible nephroscope toward the kidney using a robotic arm is also investigated in [240].

Table 2 summarizes the main strategies proposed to assist surgeons during ultrasound-guided tool insertion and steering, from mechanical and visual guides to fully robotic systems. In most of these methods, a robot autonomously steers the tool using precise measurements of the tool's shaft position. Consequently, the tool imaging methods discussed in Section 3.5 are directly applicable here, further emphasizing the critical role of accurate imaging for procedural accuracy. Using these methods, image-based or tracker-based closed-loop control algorithms employ direct image features, such as bright lines, tip shadows, and speckle patterns, or spatial information from the tracking sensor, to generate corrections to robot motion in real-time. More advanced needle insertion robotic systems combine needle and probe control in a unified setup for better visualization. These systems will be discussed in the following subsections.

4.2. *Robotic Assistance for Ultrasound Probe Control*

Precise control of an ultrasound probe mounted on a robotic arm for tool and organ imaging is one of the most studied areas in medical robotics [61, 231, 250–252]. In their simplest form, these systems have been used to autonomously or semi-autonomously image a desired organ, including, but not limited to, the liver, lung, breast, carotid artery, spine, kidney, and prostate [251]. Robotic imaging can decrease procedural complexity and overcome operator-dependent limitations [231, 253–255]. In [256–260], robotic assistance is used to automatically scan carotid arteries, the liver, the abdominal area, and the fetus. Robotic assistance for 3D ultrasound imaging is also reported in [261–265] to provide precise and repeatable probe positioning. Housden *et al.* reported dual-probe robotic setups and standardized acquisition workflows to ensure repeatable volumetric reconstructions from ultrasound scans [266].

More advanced systems keep the surgical tool in the images by automatically adjusting the position and orientation of the robot arm holding the ultrasound transducer [16, 21, 185, 239, 241, 267]. A key challenge is to simultaneously control probe position, probe orientation, and probe-tissue contact to maintain optimal image quality and target visibility.

To ensure acoustic coupling between the tissue and the ultrasound probe, force and torque sensors are commonly used in impedance/force controllers to maintain tissue contact while adapting to its anatomy [217, 267–269]. However, force sensors are usually expensive and noisy, and the measured force varies with sensor orientation and probe weight, requiring precise online calibration [270, 271]. Furthermore, force control along the ultrasound probe's longitudinal axis usually does not take into account the resulting image quality [272–274]. In most systems, the scanning path must be planned manually, with no room for real-time adjustments [258, 265]. In practice, the body surface is uneven, and it is desirable to orient the probe orthogonally to the surface.

In more advanced approaches, an initial path is derived from preoperative images and then adjusted during the procedure. Adjustment methods include trajectory planning with surface perception [275], pose estimation using RGB-D cameras [256, 257, 261–264, 276], patient-to-MRI registration [264, 277], and contact posture estimation with optical waveguide force sensors [278]. In parallel, different methods can also adjust the tissue-probe contact force during scanning. Examples include a passive spring-based mechanism that pushes the probe against the tissue [259], online optimization to determine the local tissue normal [270], re-

inforcement learning [279], and task-space compliance control [280]. Chatelain *et al.* developed a control law that regulates probe force to preserve image quality metrics and demonstrated improved image consistency [215, 281].

Like many other domains, advances in deep learning have enhanced robotic-assisted ultrasound imaging. For example, Abhimanyu *et al.* combine robot control and learning approaches to autonomously reach desired scan planes and adapt them to anatomical variability [282]. The imitation-learning method in [283] calculates the probe/tissue contact force by training a robotic controller on sonographer demonstrations to replicate the same imaging quality. Leveraging more advanced learning models, Zhang *et al.* proposed a new mapping and localization method for autonomous ultrasound imaging that does not require specific tissue features [284]. The ultrasound probe can also be controlled to move along the pre-defined path the tool is expected to take to keep the tool visible in the images [285].

The most advanced group of robotic systems for ultrasound imaging leverages vision- or tracker-based approaches introduced in Section 3.5 to estimate the position of the tool and then move the imaging probe such that the tool aligns with the imaging plane [16, 21, 185, 239, 241]. For example, optical flow is used in [185] to segment a cannula from 2D ultrasound images and translate the probe to keep it centred in the image. Many recent works have also integrated variations of neural networks or U-Net architectures to reconstruct the needle shape from ultrasound frames, estimate the position and pose of the tool tip, and use this information for closed-loop control. Lee *et al.* integrated a U-Net needle detection algorithm with an actuated probe to track the needle shape and reconstruct a 3D image of the tool in the tissue [286]. These methods require accurate registration of different reference frames to describe the position of the tissue, robot, tool, and probe in a common coordinate system, which is challenging in many cases. Automated calibration algorithms can be used to obtain these spatial relationships before the procedure begins [287, 288].

To control the robot arm holding the ultrasound probe using only real-time ultrasound images, different variations of visual servoing have been developed. In visual servoing, visual features are defined to quantify the content of the image. The speed of the imaging sensor is then controlled to minimize the error between the current and the desired image features. The relation between the time derivatives of features and the speed of the imaging probe is given by an interaction matrix, which contains the partial derivatives of the selected image features with respect to the speed of each DOF of the imaging sensor [289].

For example, in [293], visual servoing is combined with ultrasound imaging to position a robot-actuated needle in the image plane during percutaneous cholecystostomy. In [281,298], visual servoing is used to adjust the in-plane rotation for image quality optimization, and to scan peripheral arteries in [294]. Haxthausen *et al.* show the feasibility of using visual servoing with 2D ultrasound for semi-automated scanning of peripheral arteries [294]. In [295], model-free visual servoing is used to actuate a robot-controlled ultrasound probe to image a desired cross-section of a static target. Nadeau *et al.* use graph-cut segmentation of three orthogonal ultrasound images to extract image features from a target [189]. A robot arm then controls the in-plane motion of the ultrasound probe in the three orthogonal image planes to image the target. In all these examples, the position of the ultrasound probe is controlled to image a static target; that is, visual servoing is used for autonomous imaging rather than for real-time tracking. However, during most ultrasound-guided percutaneous procedures, the target (i.e., the needle) moves relative to the probe as the needle is steered toward the internal organ. In [298], visual servoing was used for needle tracking using longitudinal US images of a needle subjected to out-of-plane motion. While 3D ultrasound images may also be used to track the moving needle, 3D ultrasound is more complex than 2D, has a much lower frame rate, and may not be suitable for real-time needle steering [84, 255].

A key consideration in visual servoing is the choice of visual features. Nadeau *et al.* proposed a method where the intensity of ultrasound image pixels is directly used as an image feature to control the 6-DOF robot holding the probe [217]. Image moments have been introduced as useful features for camera-based visual servoing [299], and Green's theorem was used to find an analytical solution to the interaction matrix. Mebarki *et al.* followed with the first application of visual servoing with image moments derived from 2D ultrasound images [295, 300], where an analytical derivation of the interaction matrix with online parameter estimation was proposed to control the 6-DOF robot arm holding an ultrasound probe to image a cross-section of a static object. With a similar approach, image moments derived from 2D ultrasound images were used in [267] to track a needle in the image. In addition, [189] presented a new set of image features taken from three orthogonal ultrasound images, which provided global controller convergence even when considering symmetric objects.

Automated probe control has also been combined with robotic needle insertion using various dual-robot systems, where one robot manipulates the ultrasound probe to track the needle inserted by the other [21, 239, 241, 296, 297]. In some approaches, the robot orients the probe to acquire an optimal view of the target before inserting the needle [290–292] while other methods pre-align the needle with the desired imaging plane and only then proceed with insertion [291]. Lin *et al.* propose an ultrasound scanning robot with a 2D puncture system attached to the probe [237,292]. First, the system scans the tissue to identify the optimal puncture path from the reconstructed volume. The optimal path is then mapped to the 2D ultrasound image, and the robot punctures the tissue along the calculated path.

While a fully autonomous dual-robot system can improve precision, it removes the operator from the loop and poses safety risks, particularly given the sensitivity of image-guided algorithms to the artifacts, noise, and unexpected anatomical variations discussed in the previous sections. Table 3 summarizes these different levels of robotic

Table 3. Summary of robot-assisted ultrasound probe control strategies in increasing order of complexity

Method	Principle	Advantages	Limitations
Organ scanning	Robot images organ at fixed position [231, 253–255].	Operator-independent; standardized acquisition.	Safety hazards; anatomical variability reduces reproducibility; sensor complexity.
Volumetric reconstruction	Robot scans tissue to reconstruct volumetric image [266].	High-quality reproducible volumes; improves planning and navigation.	Requires calibration and position data; hardware complexity.
Trajectory following	Probe follows a preplanned trajectory to keep tool visible [285].	Maintains tool visualization; reduces operator workload.	Needs preplanned path; no online corrections.
Integrated probe-needle positioning	Probe positioning with needle guide for puncture [237, 290–292].	Unifies imaging and insertion; optimal puncture site and execution in single workflow.	Probe/inserter calibration required; movement is limited; no tracking inside tissue.
Visual servoing	Robot manipulates the probe to keep the target in the image [189, 217, 281, 293–295].	Closed-loop without pre-defined path.	Sensitive to image noise.
Dual-robot framework	One robot handles tool imaging; the other inserts the tool [21, 239, 241, 296, 297].	Closed-loop imaging/insertion coordination; improves accuracy and consistency.	Increased system complexity; no human in the loop; safety challenges.

assistance for probe control and tool steering.

4.3. *Teleoperation and Cooperative Control*

Robot teleoperation and cooperative human-robot control combine human expertise with robotic precision, allowing clinicians to retain decision authority while the robot smooths motions, enforces virtual fixtures, constrains trajectories, or performs fine adjustments [231, 301]. In a teleoperated system, the robotic agents are controlled from a joystick that the user operates. These systems are designed within three frameworks, i.e., unilateral teleoperation, bilateral teleoperation, and collaborative/shared control. These frameworks differ in the presence or absence of force feedback, and in the degree of autonomy granted to the teleoperated robot [252, 302, 303].

One of the most studied uses of teleoperated robotic systems in these procedures is ultrasound imaging [252, 304, 305] and tool manipulation [306–311]. The most successful example of the latter is the da Vinci system from Intuitive Surgical, which has become the clinical standard of minimally invasive surgery across a wide range of non-ultrasound-based (camera-based) laparoscopic procedures [312].

In unilateral teleoperation, the slave robot (surgical robot) follows the position or speed commands of the master device (joystick), and the operator does not receive any force feedback [313–316]. Examples of unilateral teleoperation for ultrasound imaging are provided in [313–317]. Another study presented in [121] employed augmented reality to enhance realism. More recently, Lauretti *et al.* presented a teleoperated system for percutaneous nephrolithotomy capable of online path refinements [306]. The primary drawback of unilateral teleoperation is the lack of force feedback, which prevents the operator from perceiving interaction forces with the patient, reducing both safety and task performance.

In bilateral teleoperation, forces exchanged between the surgical robot and its environment are relayed back to the operator via force feedback applied at the joystick level [317–321]. The force feedback offers the operator a more realistic sense of interaction with the teleoperated environment [252, 310, 322]. This can be accomplished by installing force sensors between each surgical robot and its tools and by relying on the measured forces to the master device. Although less applicable in robotic surgery, force feedback can also be estimated from deviations between the desired and actual positions or velocities of the slave robot, which often result from the environment's impedance, including tissue stiffness, damping, and contact constraints present at the surgical site.

The systems proposed in [317–321] used bilateral teleoperation for ultrasound imaging. Others have also developed sensorless haptic feedback using force estimators [310, 323]. Bilateral teleoperation is also widely used for tissue manipulation. For instance, Aggravi *et al.* present a bilateral teleoperation system for steering a flexible needle under 3D ultrasound image guidance [307]. The system provides the operator with a combination of kinaesthetic and vibrotactile feedback to mimic the needle/tissue-cutting force. While this framework can improve the operator's perception of the surgical site, communication delays and quantization of time and position are known sources of potential instability [252, 315, 324].

In collaborative teleoperation/shared control, some surgical tasks are split between the robot and the operator.

Instead of simply following the user's commands, the robot integrates their inputs with information from the environment, such as the location of obstacles and targets, to assist with task execution more effectively [231,252,274,325–328]. A surgical task is often broken down into multiple subtasks, part of which is handled by the robot while the operator controls the remaining parts [329]. Gottardi *et al.* [330] proposed a real-time shared control framework that dynamically regenerates paths around obstacles to help the teleoperated robot avoid collisions. Another study explored a virtual admittance model for human-robot collaboration for soft and smooth motion scaling [331]. Mixed reality is also used with teleoperation to enhance the system's flexibility [332]. More examples are proposed in [274, 325–328].

In teleoperated ultrasound imaging, the robot holding the ultrasound probe is often controlled to ensure appropriate contact with the tissue, while the teleoperator only commands the robot to slide along the tissue's surface. Ensuring proper probe/tissue contact remains a major challenge: insufficient contact force leads to poor acoustic coupling and unclear images, while excessive force can deform the tissue unnecessarily [231, 302]. A dedicated force controller is commonly used to limit the applied force, such as hybrid force/position controllers [276], impedance controllers [264], and admittance controllers [274, 326]. Several works have addressed this issue by comparing real-time ultrasound images with preoperative images to adjust the contact force [264, 333]. Tsumura *et al.* designed a series-elastic-actuated end-effector that acquires diagnostic images with minimal contact force [334]. Others have instead used ultrasound image features, such as image quality metrics, to optimize contact during scanning [173, 256, 257, 260, 265, 277, 335, 336].

Shared control is also useful in addressing target motion and tissue deformation, using, for example, viscoelastic models of the tool and tissue contact to estimate tissue motion [309, 337]. For instance, the teleoperated needle insertion system in [308] uses a model to compensate for respiratory motion during liver biopsy.

Table 4 summarizes these three different teleoperation and shared control frameworks for ultrasound scanning and tool manipulation. While teleoperation promises enhanced operational capabilities, it requires robust implementation to handle communication latency, provide transparent haptic feedback tailored to specific applications, and ensure operational safety before deployment. Some systems have reached clinical or *in-vivo* stages, but clinical adoption remains limited [231, 252, 338]. The limitations summarized in Table 4 explain part of these barriers. On the control side, bilateral systems remain sensitive to communication delay, which affects both stability and accuracy; cooperative systems depend on robust sensing and communication and accurate models identified for a given task and tissue, such as the respiratory model used for liver biopsy in [308]; while unilateral systems, on the other hand, provide no force information, so the operator perceives tissue only through the image. On the workflow side, these systems add hardware to the patient table, require setup and calibration time, and must allow the interventionist to take over at any point. These barriers, and those that apply to the other levels of assistance, are discussed in Section 5.3.

5. Discussion and Conclusion

Ultrasound-guided percutaneous interventions offer a balance of real-time imaging, safety, and accessibility, yet it remains a technically demanding form of image-guided surgery. This section summarizes the challenges that motivate the need for robotic assistance, reviews what each level of assistance provides, and examines remaining limitations.

5.1. *Overview of Challenges and Assistance Levels*

The challenges of ultrasound-guided percutaneous interventions can be primarily attributed to inherent limitations of ultrasound imaging, including speckle noise, acoustic shadowing, reverberations, and sensitivity to probe orientation and tissue contact. They frequently result in partial or inconsistent visualization of anatomical targets and surgical tools. These challenges are further exacerbated by the need for precise coordination between probe manipulation and tool steering, making guidance accuracy highly dependent on operator expertise. In deep or anatomically complex regions, a limited field of view, out-of-plane tool motion, and dynamic tissue deformation further degrade visibility and increase procedural uncertainty. Together, these factors result in a high cognitive workload, variability in procedural outcomes, and a steep learning curve. These fundamental challenges are interdependent: reduced imaging quality degrades the accuracy and stability of tool and probe manipulation, while suboptimal manipulation further compromises image quality, reinforcing the cycle.

A wide range of methods has been proposed to enhance the reliability and usability of ultrasound-guided percutaneous interventions. From a system standpoint, we categorized them into three complementary levels of assistance. At the image level, signal processing and learning-based techniques aim to improve image quality and suppress noise and artifacts, thereby enhancing tissue visibility and stabilizing downstream processing. At the perceptual level, several methods seek to improve the operator's understanding of anatomical structures and tool location within the ultrasound field of view, including image segmentation, image registration, image fusion, and data augmentation. At the interventional level, robotic and algorithmic assistance focuses on tool navigation and probe control, enabling more precise targeting, improved visualization, and reduced operator burden. Collectively, these approaches reflect a shift from isolated image improvement toward integrated perception and control strategies that support both human decision-making and automated assistance during ultrasound-guided percutaneous interventions.

Table 4. Summary of teleoperation and cooperative control in robot-assisted ultrasound and tool manipulation

Method	Principle	Advantages	Limitations
Unilateral (no force feedback)	Operator commands slave robot without force feedback. [313–317].	Simple, stable, suitable for telemedicine; low complexity.	No force feedback/tissue perception; safety and image coupling issues.
Bilateral (with force feedback)	Patient/robot forces displayed to operator as haptic feedback [310, 317–321, 323].	Improves accuracy of scanning and tool insertion [307]; enables micromanipulation; safer tissue contact.	Communication delay; potential instability; expensive hardware; safety hazards.
Cooperative control	Robot and human share tasks [274, 308, 309, 325–328, 330, 331].	Stabilized, scaled motion and force, motion compensation; human in the loop; safer.	Requires robust sensing; challenging controller tuning; limited user acceptance.

5.2. *Persistent Technical Limitations*

Despite substantial progress across all three assistance levels, several limitations persist. Image enhancement methods alone cannot guarantee reliable visibility in the presence of artifacts or suboptimal probe–tool alignment. Image interpretation methods, such as segmentation and registration, often rely on assumptions about image quality, anatomy, or tool appearance that may not hold across different patients or procedures. Interventional assistance strategies, including robotic guidance and visual servoing, remain sensitive to partial observability, out-of-plane tool motion, and delays or inaccuracies in image-based feedback. Moreover, many proposed systems depend on external tracking devices, preoperative planning, or extensive calibration, which increases setup complexity and limits robustness in real clinical environments. These observations highlight that no single level of assistance is sufficient on its own and that effective ultrasound-guided percutaneous interventions require tighter integration between image quality enhancement, perceptual interpretation, and control strategies.

5.3. *Barriers to Clinical Translation*

This section gives a general perspective on the barriers between research prototypes and clinical use, based on the literature reviewed in this paper, and is not a complete account of the topic. Most of the works covered in this review report technical validation rather than clinical use. Methods are evaluated on recorded ultrasound images, in phantoms, or in *ex vivo* tissue, and the reported metrics describe accuracy under controlled conditions. A smaller number report studies in patients. For example, electromagnetic needle tracking has been compared with freehand insertion in [123, 203, 205]. Another example is the randomized trial reported in [229], which compared robot-assisted renal access with manual ultrasound-guided access for percutaneous nephrolithotomy. The same pattern appears in surveys of robotic ultrasound systems, confirming that the gap between research progress and clinical use has not narrowed at the same rate as technical progress [231, 252, 338–340]. We therefore found it not possible to assign a level of clinical readiness to each method discussed in this review. The review covers representative examples rather than a complete coverage of the literature, and reports validation under different conditions. A systematic evaluation of clinical evidence would require a dedicated study with predefined inclusion criteria.

Operating room deployment presents other barriers. Robotic systems add equipment to a workspace that is already constrained, which affects access to the patient and the position of the clinical team. Sterility requirements limit the design of the system. Setup, registration, and calibration add time to the procedure, and this time is difficult to recover during the intervention. Registration accuracy also degrades with patient motion, breathing, and tissue deformation, so the alignment established before insertion does not hold throughout the procedure. Systems that need external tracking devices are further affected by line-of-sight constraints and by field distortion. The interventionist must also be able to take over the task at any point, which requires a clear transfer of control and adds training requirements [339, 340].

The evidence available for these systems is limited for methodological reasons as well. Studies are often conducted on small cohorts and in a single centre, and accuracy is reported with different metrics, different phantoms, and different targets, making it difficult to compare results across studies. Shared datasets and benchmarks are not widely available, which limits reproducibility. Moreover, systems that apply closed-loop control to a robot that contacts the patient face a higher regulatory burden than systems that only process images, and this affects how quickly they can move to clinical evaluation.

5.4. *Future Directions and Conclusion*

Future research in ultrasound-guided percutaneous interventions may focus on integrated frameworks that jointly address image quality, image interpretation, and interventional assistance under practical clinical constraints.

Promising directions include uncertainty-aware imaging and control methods that explicitly account for variable image reliability, approaches capable of robustly handling out-of-plane tool motion and dynamic tissue deformation, and tighter coupling between perception and control to enable adaptive, image-driven assistance in real time. Equally important are human-centred designs that support shared autonomy, preserve the interventionist's authority, and reduce cognitive workload without compromising safety or flexibility. A systematic review of clinical outcomes and levels of evidence for the systems discussed here would complement the technical perspective of this paper.

This paper reviewed methods that address the limitations of ultrasound-guided percutaneous interventions, organized along three levels of assistance ranging from image processing algorithms to interventional robotic systems. The review shows that the main challenges are interdependent and that no single level of assistance resolves them alone. Addressing these challenges is essential for translating recent advances into clinically deployable systems and for enabling wider adoption of ultrasound-guided percutaneous interventions in routine practice.

Acknowledgments

We acknowledge the support of the Natural Sciences and Engineering Research Council of Canada (NSERC), [funding reference number RGPIN-2025-05468]. Cette recherche a été financée par le Conseil de recherches en sciences naturelles et en génie du Canada (CRSNG), [no. de référ. RGPIN-2025-05468].

References

[1] M. M. Siddiqui, S. Rais-Bahrami, B. Turkbey *et al.*, Comparison of MR/ultrasound fusion–guided biopsy with ultrasound-guided biopsy for the diagnosis of prostate cancer, *JAMA* **313**(4) (2015) 390–397.

[2] T. Helbich, W. Matzek, M. Fuchsjäger, Stereotactic and ultrasound-guided breast biopsy, *European Radiology* **14**(3) (2004) 383–393.

[3] A. Hakime, S. Yevich, L. Tselikas *et al.*, Percutaneous thermal ablation with ultrasound guidance. fusion imaging guidance to improve conspicuity of liver metastasis, *Cardiovascular and Interventional Radiology* **40**(5) (2017) 721–727.

[4] Y. Minami, M. Kudo, Ultrasound fusion imaging technologies for guidance in ablation therapy for liver cancer, *Journal of Medical Ultrasonics* **47**(2) (2020) 257–263.

[5] D. Lyrdal, M. Andersson, M. Hellström *et al.*, Ultrasound-guided percutaneous radiofrequency ablation of small renal tumors: Clinical results and radiological evolution during follow-up, *Acta Radiologica* **51**(7) (2010) 808–818.

[6] B. Lojanapiwat, The ideal puncture approach for PCNL: Fluoroscopy, ultrasound or endoscopy?, *Indian Journal of Urology* **29**(3) (2013) p. 208.

[7] F. C. Ng, W. L. Yam, T. Y. B. Lim *et al.*, Ultrasound-guided percutaneous nephrolithotomy: Advantages and limitations, *Investigative and Clinical Urology* **58**(5) (2017) 346–352.

[8] F. Darmoch, M. C. Alraies, Y. Al-Khadra *et al.*, Intravascular ultrasound imaging–guided versus coronary angiography–guided percutaneous coronary intervention: A systematic review and meta-analysis, *Journal of the American Heart Association* **9**(5) (2020) p. e013678.

[9] M. Ahmed, L. Solbiati, C. L. Brace *et al.*, Image-guided tumor ablation: Standardization of terminology and reporting criteria—a 10-year update, *Radiology* **273**(1) (2014) 241–260.

[10] D. Filippiadis, G. Mauri, P. Marra *et al.*, Percutaneous ablation techniques for renal cell carcinoma: Current status and future trends, *International Journal of Hyperthermia* **36**(2) (2019) 21–30.

[11] A. Greene, R. Young, C. Rainey *et al.*, Computed tomography, ultrasound and fluoroscopy guidance in intra-articular sacroiliac joint injections: A systematic review, *Radiography* **32**(4S1) (2026) p. 103332.

[12] A. U. Kishan, T. M. Ma, J. M. Lamb *et al.*, Magnetic resonance imaging–guided vs computed tomography–guided stereotactic body radiotherapy for prostate cancer: The MIRAGE randomized clinical trial, *JAMA Oncology* **9**(3) (2023) 365–373.

[13] M. Corrales, S. Doizi, Y. Barghouthy *et al.*, Ultrasound or fluoroscopy for percutaneous nephrolithotomy access, is there really a difference? A review of literature, *Journal of Endourology* **35**(3) (2021) 241–248.

[14] R. M. Geraghty, N. F. Davis, L. Tzelves *et al.*, Best practice in interventional management of urolithiasis: An update from the european association of urology guidelines panel for urolithiasis 2022, *European Urology Focus* **9**(1) (2023) 199–208.

[15] D. T. Tzou, T. O. Tailly, K. L. Stern, Ultrasound-guided PCNL–why are we still performing exclusively fluoroscopic access?, *Current Urology Reports* **24**(7) (2023) 335–343.

[16] M. Pavone, B. Seeliger, E. Teodorico *et al.*, Ultrasound-guided robotic surgical procedures: A systematic review, *Surgical Endoscopy* **38**(5) (2024) 2359–2370.

[17] S. H. C. Ortiz, T. Chiu, M. D. Fox, Ultrasound image enhancement: A review, *Biomed. Signal Process. Control* **7**(5) (2012) 419–428.

[18] G. Reusz, P. Sarkany, J. Gal *et al.*, Needle-related ultrasound artifacts and their importance in anaesthetic practice, *British Journal of Anaesthesia* **112**(5) (2014) 794–802.

[19] J. Huang, J. K. Triedman, N. V. Vasilyev *et al.*, Imaging artifacts of medical instruments in ultrasound-guided interventions, *Journal of Ultrasound in Medicine* **26**(10) (2007) 1303–1322.

[20] S.-C. Liao, S.-C. Shao, S.-Y. Gao *et al.*, Augmented reality visualization for ultrasound-guided interventions: a pilot randomized crossover trial to assess trainee performance and cognitive load, *BMC Medical Education* **24**(1) (2024) p. 1058.

[21] Y. Li, Z. Lu, A. Tzemanaki *et al.*, An ultrasound visual servoing dual-arm robotics system for needle placement in brachytherapy treatment, *Frontiers in Robotics and AI* **12** (2025) p. 1558182.

[22] A. I. of Ultrasound in Medicine *et al.*, AIUM practice principles for work-related musculoskeletal disorder, *Journal of Ultrasound in Medicine* **42**(5) (2023) 1139–57.

[23] M. Usawachintachit, S. Masic, I. E. Allen *et al.*, Adopting ultrasound guidance for prone percutaneous nephrolithotomy: Evaluating the learning curve for the experienced surgeon, *Journal of Endourology* **30**(8) (2016) 856–863.

[24] P. Alken, Percutaneous nephrolithotomy–the puncture, *BJU International* **129**(1) (2022) 17–24.

[25] C. Che, T. S. Mathai, J. Galeotti, Ultrasound registration: A review, *Methods* **115** (2017) 128–143.

[26] C. A. Duarte-Salazar, A. E. Castro-Ospina, M. A. Becerra *et al.*, Speckle noise reduction in ultrasound images for improving the metrological evaluation of biomedical applications: An overview, *IEEE Access* **8** (2020) 15983–15999.

[27] S. K. Pal, A. Bhardwaj, A. Shukla, A review on despeckling filters in ultrasound images for speckle noise reduction, *2021 International Conference on Advance Computing and Innovative Technologies in Engineering (ICACITE)*, IEEE (2021), pp. 973–978.

[28] O. V. Michailovich, A. Tannenbaum, Despeckling of medical ultrasound images, *IEEE Transactions on Ultrasonics, Ferroelectrics, and Frequency Control* **53**(1) (2006) 64–78.

[29] S. Finn, M. Glavin, E. Jones, Echocardiographic speckle reduction comparison, *IEEE Transactions on Ultrasonics, Ferroelectrics, and Frequency Control* **58**(1) (2011) 82–101.

[30] R. Rosa, F. C. Monteiro, Performance analysis of speckle ultrasound image filtering, *Computer Methods in Biomechanics and Biomedical Engineering: Imaging & Visualization* **4**(3-4) (2016) 193–201.

[31] K. Singh, S. K. Ranade, C. Singh, A hybrid algorithm for speckle noise reduction of ultrasound images, *Computer Methods and Programs in Biomedicine* **148** (2017) 55–69.

[32] J. Zhang, C. Wang, Y. Cheng, Comparison of despeckle filters for breast ultrasound images, *Circuits, Systems, and Signal Processing* **34**(1) (2015) 185–208.

[33] C. Lopez-Molina, M. Galar, H. Bustince *et al.*, On the impact of anisotropic diffusion on edge detection, *Pattern Recognition* **47**(1) (2014) 270–281.

[34] J. L. Mateo, A. Fernández-Caballero, Finding out general tendencies in speckle noise reduction in ultrasound images, *Expert Systems with Applications* **36**(4) (2009) 7786–7797.

[35] S. T. Acton, Deconvolutional speckle reducing anisotropic diffusion, *IEEE International Conference on Image Processing 2005*, **1**, IEEE (2005), pp. I–5.

[36] S. Aja-Fernández, C. Alberola-López, On the estimation of the coefficient of variation for anisotropic diffusion speckle filtering, *IEEE Transactions on Image Processing* **15**(9) (2006) 2694–2701.

[37] S. Balocco, C. Gatta, O. Pujol *et al.*, SRBF: Speckle reducing bilateral filtering, *Ultrasound in Medicine & Biology* **36**(8) (2010) 1353–1363.

[38] C. Chinrungrueng, A. Suvichakorn, Fast edge-preserving noise reduction for ultrasound images, *IEEE Transactions on Nuclear Science* **48**(3) (2001) 849–854.

[39] J. Xu, Y. Jia, Z. Shi *et al.*, An improved anisotropic diffusion filter with semi-adaptive threshold for edge preservation, *Signal Processing* **119** (2016) 80–91.

[40] S. Sudha, G. Suresh, R. Sukanesh, Speckle noise reduction in ultrasound images by wavelet thresholding based on weighted variance, *International Journal of Computer Theory and Engineering* **1**(1) (2009) p. 7.

[41] J. Yang, J. Fan, D. Ai *et al.*, Local statistics and non-local mean filter for speckle noise reduction in medical ultrasound image, *Neurocomputing* **195** (2016) 88–95.

[42] P. C. Tay, C. D. Garson, S. T. Acton *et al.*, Ultrasound despeckling for contrast enhancement, *IEEE Transactions on Image Processing* **19**(7) (2010) 1847–1860.

[43] D. Vilimek, J. Kubicek, M. Golian *et al.*, Comparative analysis of wavelet transform filtering systems for noise reduction in ultrasound images, *PLOS ONE* **17**(7) (2022) p. e0270745.

[44] Q. Huang, F. Zhang, X. Li, Machine learning in ultrasound computer-aided diagnostic systems: A survey, *BioMed Research International* **2018**(1) (2018) p. 5137904.

[45] D. Mishra, S. Tyagi, S. Chaudhury *et al.*, Despeckling CNN with ensembles of classical outputs, *2018 24th International Conference on Pattern Recognition (ICPR)*, IEEE (2018), pp. 3802–3807.

[46] A. Dubey, H. Uldin, Z. Khan *et al.*, Role of artificial intelligence in musculoskeletal interventions, *Cancers* **17**(10) (2025) p. 1615.

[47] D. Perdios, M. Vonlanthen, A. Besson *et al.*, Deep convolutional neural network for ultrasound image enhancement, *2018 IEEE International Ultrasonics Symposium (IUS)*, IEEE (2018), pp. 1–4.

[48] S. Cammarasana, P. Nicolardi, G. Patanè, Real-time denoising of ultrasound images based on deep learning, *Medical & Biological Engineering & Computing* **60**(8) (2022) 2229–2244.

[49] H. Kang, C. Park, H. Yang, Evaluation of denoising performance of resnet deep learning model for ultrasound images corresponding to two frequency parameters, *Bioengineering* **11**(7) (2024) p. 723.

[50] D. Jung, M. Kang, S. H. Park *et al.*, Unsupervised

speckle noise reduction technique for clinical ultrasound imaging, *Ultrasonography* **43**(5) (2024) 327–344.

[51] K. Song, J. Feng, D. Chen, A survey on deep learning in medical ultrasound imaging, *Frontiers in Physics* **12** (2024) p. 1398393.

[52] H. Asgariandehkordi, S. Goudarzi, M. Sharifzadeh *et al.*, Denoising plane wave ultrasound images using diffusion probabilistic models, *IEEE Transactions on Ultrasonics, Ferroelectrics, and Frequency Control* **71**(11) (2024) 1526–1539.

[53] T. S. W. Stevens, F. C. Meral, J. Yu *et al.*, Dehazing ultrasound using diffusion models, *IEEE Transactions on Medical Imaging* **43**(10) (2024) 3546–3558.

[54] Y. Hu, H. Xu, X. Zhu *et al.*, An exploratory study on ultrasound image denoising using feature extraction and adversarial diffusion model, *Medical Physics* **52**(10) (2025) p. e70023.

[55] J. Liu, C. Li, L. Liu *et al.*, Speckle noise reduction for medical ultrasound images based on cycle-consistent generative adversarial network, *Biomedical Signal Processing and Control* **86** (2023) p. 105150.

[56] X. Li, N. Navab, Z. Jiang, Speckle2Self: Self-supervised ultrasound speckle reduction without clean data, *Medical image analysis* (2025) p. 103755.

[57] C. Oulmalme, H. Nakouri, F. Jaafar, A systematic review of generative AI approaches for medical image enhancement: Comparing GANs, transformers, and diffusion models, *International journal of medical informatics* **199** (2025) p. 105903.

[58] M. Z. Degu, M. Madhusoodanan, M. Chippa *et al.*, Scoping review of recent trends and challenges in artificial intelligence based medical ultrasound denoising, *AI in Medicine* **1**(3) (2026) p. 18.

[59] E. Smistad, K. F. Johansen, D. H. Iversen *et al.*, Highlighting nerves and blood vessels for ultrasound-guided axillary nerve block procedures using neural networks, *Journal of Medical Imaging* **5**(4) (2018) 044004–044004.

[60] P. F. Müller, D. Schlager, S. Hein *et al.*, Robotic stone surgery–current state and future prospects: A systematic review, *Arab Journal of Urology* **16**(3) (2018) 357–364.

[61] F. Ferraguti, S. Farsoni, M. Bonfè, Augmented reality and robotic systems for assistance in percutaneous nephrolithotomy procedures: Recent advances and future perspectives, *Electronics* **11**(19) (2022) p. 2984.

[62] V. Gauhar, C. Giulioni, N. Gadzhiev *et al.*, An update of in vivo application of artificial intelligence and robotics for percutaneous nephrolithotripsy: Results from a systematic review, *Current Urology Reports* **24**(6) (2023) 271–280.

[63] N. Gadzhiev, I. Semeniakin, A. Morshnev *et al.*, Role and utility of mixed reality technology in laparoscopic partial nephrectomy: outcomes of a prospective RCT using an indigenously developed software, *Advances in Urology* **2022**(1) (2022) p. 8992051.

[64] Y. Xu, Y. Wang, J. Yuan *et al.*, Medical breast ultrasound image segmentation by machine learning, *Ultrasonics* **91** (2019) 1–9.

[65] Q. Huang, Y. Luo, Q. Zhang, Breast ultrasound image segmentation: A survey, *International Journal of Computer Assisted Radiology and Surgery* **12**(3) (2017) 493–507.

[66] S. Hussain, X. Xi, I. Ullah *et al.*, Contextual level-set method for breast tumor segmentation, *IEEE Access* **8** (2020) 189343–189353.

[67] N. Karunanayake, W. Lohitvisate, S. S. Makhanov, Artificial life for segmentation of fusion ultrasound images of breast abnormalities, *Pattern Recognition* **131** (2022) p. 108838.

[68] Y.-L. Huang, Y.-R. Jiang, D.-R. Chen *et al.*, Level set contouring for breast tumor in sonography, *Journal of Digital Imaging* **20**(3) (2007) 238–247.

[69] L. Cai, Q. Li, J. Zhang *et al.*, Ultrasound image segmentation based on transformer and U-Net with joint loss, *PeerJ Computer Science* **9** (2023) p. e1638.

[70] B. Sainsbury, O. Wilz, J. Ren *et al.*, Preoperative virtual reality surgical rehearsal of renal access during percutaneous nephrolithotomy: A pilot study, *Electronics* **11**(10) (2022) p. 1562.

[71] D. Veneziano, A. Smith, T. Reihsen *et al.*, The SimPORTAL fluoro-less C-arm trainer: An innovative device for percutaneous kidney access, *Journal of Endourology* **29**(2) (2015) 240–245.

[72] Y. A. Asaye, P. Annamalai, L. G. Ayalew, Detection of kidney stone from ultrasound images using machine learning algorithms, *Scientific African* **28** (2025) p. e02618.

[73] T. Borges, A. Rai, D. Raj *et al.*, Kidney stone detection using ultrasound images, *Proceedings of the Advancement in Electronics & Communication Engineering* (2022).

[74] R. Goel, A. Jain, Improved detection of kidney stone in ultrasound images using segmentation techniques, *Advances in Data and Information Sciences: Proceedings of ICDIS 2019*, (Springer, 2020), pp. 623–641.

[75] K. Viswanath, R. Gunasundari, S. A. Hussan, VLSI implementation and analysis of kidney stone detection by level set segmentation and ANN classification, *Procedia Computer Science* **48** (2015) 612–622.

[76] R. A. Raja, J. J. Ranjani, Segment based detection and quantification of kidney stones and its symmetric analysis using texture properties based on logical operators with ultrasound scanning, *International Journal of Computer Applications* **975** (2013) p. 8887.

[77] S. H. Song, J. H. Han, K. S. Kim *et al.*, Deep-learning segmentation of ultrasound images for automated calculation of the hydronephrosis area to renal parenchyma ratio, *Investigative and Clinical Urology* **63**(4) (2022) p. 455.

[78] K. Viswanath, B. Anilkumar, R. Gunasundari, Design of deep learning reaction–diffusion level set seg-

mentation approach for health care related to automatic kidney stone detection analysis, *Multimedia Tools and Applications* **81**(29) (2022) 41807–41849.

[79] S. Gite, A. Mishra, K. Kotecha, Enhanced lung image segmentation using deep learning, *Neural Computing and Applications* **35**(31) (2023) 22839–22853.

[80] N. Jain, V. Kumar, Liver ultrasound image segmentation using region-difference filters, *Journal of Digital Imaging* **30**(3) (2017) 376–390.

[81] M. Y. Ansari, I. A. C. Mangalote, D. Masri *et al.*, Neural network-based fast liver ultrasound image segmentation, *2023 International Joint Conference on Neural Networks (IJCNN)*, (2023), pp. 1–8.

[82] J. Wu, F. Liu, W. Sun *et al.*, Boundary-aware convolutional attention network for liver segmentation in ultrasound images, *Scientific Reports* **14**(1) (2024) p. 21529.

[83] M. Khadem, C. Rossa, R. S. Sloboda *et al.*, Ultrasound-guided model predictive control of needle steering in biological tissue, *Journal of Medical Robotics Research* **1**(01) (2016) p. 1640007.

[84] H. J. Scholten, A. Pourtaherian, N. Mihajlovic *et al.*, Improving needle tip identification during ultrasound-guided procedures in anaesthetic practice, *Anaesthesia* **72**(7) (2017) 889–904.

[85] G. Xiao, M. Brady, J. A. Noble *et al.*, Segmentation of ultrasound B-mode images with intensity inhomogeneity correction, *IEEE Transactions on Medical Imaging* **21**(1) (2002) 48–57.

[86] K. Saini, M. Dewal, M. Rohit, Ultrasound imaging and image segmentation in the area of ultrasound: A review, *International Journal of Advanced Science and Technology* **24** (2010) 41–60.

[87] B. He, S. Zhao, Y. Dai *et al.*, A robust and automatic CT-3D ultrasound registration method based on segmentation, context, and edge hybrid metric, *Medical Physics* **50**(10) (2023) 6243–6258.

[88] D. Gupta, R. S. Anand, A hybrid edge-based segmentation approach for ultrasound medical images, *Biomedical Signal Processing and Control* **31** (2017) 116–126.

[89] D. Boukerroui, A. Baskurt, J. A. Noble *et al.*, Segmentation of ultrasound images—-multiresolution 2D and 3D algorithm based on global and local statistics, *Pattern Recognition Letters* **24**(4-5) (2003) 779–790.

[90] M. Nikolic, E. Tuba, M. Tuba, Edge detection in medical ultrasound images using adjusted canny edge detection algorithm, *2016 24th telecommunications forum (TELFOR)*, IEEE (2016), pp. 1–4.

[91] A. Madabhushi, D. Metaxas, Combining low-, high-level and empirical domain knowledge for automated segmentation of ultrasonic breast lesions, *IEEE Transactions on Medical Imaging* **22**(2) (2003) 155–169.

[92] M.-H. Cardinal, J. Meunier, G. Soulez *et al.*, Intravascular ultrasound image segmentation: A three-dimensional fast-marching method based on gray level distributions, *IEEE Transactions on Medical Imaging* **25**(5) (2006) 590–601.

[93] M. Gudmundsson, E. A. El-Kwae, M. R. Kabuka, Edge detection in medical images using a genetic algorithm, *IEEE Transactions on Medical Imaging* **17**(3) (1998) 469–474.

[94] U. Maulik, Medical image segmentation using genetic algorithms, *IEEE Transactions on Information Technology in Biomedicine* **13**(2) (2009) 166–173.

[95] R. Kolář, J. Kozumplík, Fuzzy approach in ultrasound image segmentation, *International Conference on Computational Intelligence*, Springer (2001), pp. 924–929.

[96] A. R. Abdel-Dayem, M. R. El-Sakka, Carotid artery ultrasound image segmentation using fuzzy region growing, *International Conference Image Analysis and Recognition*, Springer (2005), pp. 869–878.

[97] Z. Iscan, M. N. Kurnaz, Z. Dokur *et al.*, Ultrasound image segmentation by using wavelet transform and self-organizing neural network, *Neural Information Processing-Letters and Reviews* **10**(8-9) (2006) 183–191.

[98] H.-M. Wu, H. H.-S. Lu, Iterative sliced inverse regression for segmentation of ultrasound and MR images, *Pattern Recognition* **40**(12) (2007) 3492–3502.

[99] M. Kurnaz, T. Olmez, Tissue segmentation in ultrasound images by using genetic algorithms, *Expert Systems With Applications* **34** (2007) 2739–2746.

[100] M. Khouy, Y. Jabrane, M. Ameur *et al.*, Medical image segmentation using automatic optimized U-Net architecture based on genetic algorithm, *Journal of Personalized Medicine* **13**(9) (2023) p. 1298.

[101] S. Zhang, M. Liao, J. Wang *et al.*, Fully automatic tumor segmentation of breast ultrasound images with deep learning, *Journal of Applied Clinical Medical Physics* **24**(1) (2023) p. e13863.

[102] P. Wang, M. Vives, V. M. Patel *et al.*, Robust real-time bone surfaces segmentation from ultrasound using a local phase tensor-guided CNN, *International Journal of Computer Assisted Radiology and Surgery* **15**(7) (2020) 1127–1135.

[103] R. Almajalid, J. Shan, Y. Du *et al.*, Development of a deep-learning-based method for breast ultrasound image segmentation, *2018 17th IEEE International Conference on Machine Learning and Applications (ICMLA)*, IEEE (2018), pp. 1103–1108.

[104] G. Chen, L. Li, J. Zhang *et al.*, Rethinking the unpretentious U-net for medical ultrasound image segmentation, *Pattern Recognition* **142** (2023) p. 109728.

[105] L. Qian, H. Huang, X. Xia *et al.*, Automatic segmentation method using FCN with multi-scale dilated convolution for medical ultrasound image, *The Visual Computer* **39**(11) (2023) 5953–5969.

[106] M. Marsousi, K. N. Plataniotis, S. Stergiopoulos, An automated approach for kidney segmentation in three-dimensional ultrasound images, *IEEE Journal of Biomedical and Health Informatics* **21**(4) (2016) 1079–1094.

[107] X. Yang, L. Yu, S. Li *et al.*, Towards automated semantic segmentation in prenatal volumetric ultrasound, *IEEE Transactions on Medical Imaging* **38**(1) (2018) 180–193.

[108] J. Ma, Y. He, F. Li *et al.*, Segment anything in medical images, *Nature communications* **15**(1) (2024) p. 654.

[109] Y. Huang, X. Yang, L. Liu *et al.*, Segment anything model for medical images?, *Medical Image Analysis* **92** (2024) p. 103061.

[110] X. Lin, Y. Xiang, L. Yu *et al.*, Beyond adapting SAM: Towards end-to-end ultrasound image segmentation via auto prompting, *International conference on medical image computing and computer-assisted intervention*, Springer (2024), pp. 24–34.

[111] F. Tian, J. Zhai, J. Gong *et al.*, SAM-MedUS: A foundational model for universal ultrasound image segmentation, *Journal of Medical Imaging* **12**(2) (2025) 027001–027001.

[112] A. Meyer, A. Murali, F. Zarin *et al.*, Ultrasam: A foundation model for ultrasound using large open-access segmentation datasets, *International Journal of Computer Assisted Radiology and Surgery* **21**(1) (2026) 93–102.

[113] H. Chen, Y. Cai, C. Wang *et al.*, Multi-organ foundation model for universal ultrasound image segmentation with task prompt and anatomical prior, *IEEE Transactions on Medical Imaging* **44**(2) (2025) 1005–1018.

[114] B. Podvin, T. Collins, G. Saibro *et al.*, SAMUSA: Segment anything model 2 for ultrasound annotation, *International Conference on Medical Image Computing and Computer-Assisted Intervention*, Springer (2025), pp. 509–518.

[115] H. Rasaee, T. Koleilat, H. Rivaz, Grounding DINO-US-SAM: Text-prompted multiorgan segmentation in ultrasound with LoRA-tuned vision–language models, *IEEE Transactions on Ultrasonics, Ferroelectrics, and Frequency Control* **72**(10) (2025) 1414–1425.

[116] F. Darzi, T. Bocklitz, A review of medical image registration for different modalities, *Bioengineering* **11**(8) (2024) p. 786.

[117] R. R. Wildeboer, R. J. van Sloun, A. W. Postema *et al.*, Accurate validation of ultrasound imaging of prostate cancer: A review of challenges in registration of imaging and histopathology, *Journal of Ultrasound* **21**(3) (2018) 197–207.

[118] Z. Zhao, J. Poyhonen, X. Chen Cai *et al.*, Augmented reality technology in image-guided therapy: State-of-the-art review, *Proceedings of the Institution of Mechanical Engineers, Part H: Journal of Engineering in Medicine* **235**(12) (2021) 1386–1398.

[119] T. Borde, L. Saccenti, M. Li *et al.*, Smart goggles augmented reality CT–US fusion compared to conventional fusion navigation for percutaneous needle insertion, *International Journal of Computer Assisted Radiology and Surgery* **20**(1) (2025) 107–115.

[120] K. Chandelon, A. Pitout, M. Souchaud *et al.*, Landmark-free automatic digital twin registration in robot-assisted partial nephrectomy using a generic end-to-end model, *International Journal of Computer Assisted Radiology and Surgery* **20**(9) (2025) 1931–1940.

[121] Y. Fu, W. Lin, X. Yu *et al.*, Robot-assisted teleoperation ultrasound system based on fusion of augmented reality and predictive force, *IEEE Transactions on Industrial Electronics* **70**(7) (2022) 7449–7456.

[122] S. Morita, K. Suzuki, T. Yamamoto *et al.*, Out-of-plane needle placements using 3D augmented reality protractor on smartphone: An experimental phantom study, *Cardiovascular and Interventional Radiology* **46**(5) (2023) 675–679.

[123] A. Seitel, D. Groener, M. Eisenmann *et al.*, Miniaturized electromagnetic tracking enables efficient ultrasound-navigated needle insertions, *Scientific Reports* **14**(1) (2024) p. 14161.

[124] Q. Li, R. Song, X. Ma *et al.*, A robust registration algorithm for image-guided surgical robot, *IEEE Access* **6** (2018) 42950–42960.

[125] H. Qiu, C. Qin, A. Schuh *et al.*, Learning diffeomorphic and modality-invariant registration using B-splines, *Proceedings of the Fourth Conference on Medical Imaging with Deep Learning*, (2021), pp. 645–664.

[126] N. D. Cahill, Normalized measures of mutual information with general definitions of entropy for multimodal image registration, *International workshop on biomedical image registration*, Springer (2010), pp. 258–268.

[127] M. R. Sabuncu, *Entropy-based image registration* (Princeton University, 2006).

[128] M. M. Alam, T. Howlader, S. M. Rahman, Entropy-based image registration method using the curvelet transform, *Signal, Image and Video Processing* **8**(3) (2014) 491–505.

[129] M. Nanavati, M. Shah, Performance comparison of different wavelet based image fusion techniques for lumbar spine images, *Journal of Integrated Science and Technology* **12**(1) (2024) 703–703.

[130] G. Loi, M. Fusella, E. Lanzi *et al.*, Performance of commercially available deformable image registration platforms for contour propagation using patient-based computational phantoms: A multi-institutional study, *Medical Physics* **45**(2) (2018) 748–757.

[131] G. Song, J. Han, Y. Zhao *et al.*, A review on medical image registration as an optimization problem, *Current Medical Imaging* **13**(3) (2017) 274–283.

[132] M. Keil, C. Oyarzun Laura, S. Wesarg, Ultrasound B-mode segmentation for registration with CT in percutaneous hepatic interventions, *Workshop on Clinical Image-Based Procedures*, Springer (2012), pp. 91–97.

[133] D. Lee, W. H. Nam, J. Y. Lee *et al.*, Non-rigid registration between 3d ultrasound and CT images of the liver based on intensity and gradient informa-

tion, *Physics in Medicine and Biology* **56**(1) (2011) 117–137.

[134] W. Wein, S. Brunke, A. Khamene *et al.*, Automatic CT-ultrasound registration for diagnostic imaging and image-guided intervention, *Medical Image Analysis* **12**(5) (2008) 577–585.

[135] C. X. Yan, B. Goulet, J. Pelletier *et al.*, Towards accurate, robust and practical ultrasound-CT registration of vertebrae for image-guided spine surgery, *International Journal of Computer Assisted Radiology and Surgery* **6**(4) (2011) 523–537.

[136] L. Gong, H. Wang, C. Peng *et al.*, Non-rigid MR-TRUS image registration for image-guided prostate biopsy using correlation ratio-based mutual information, *BioMedical Engineering OnLine* **16**(1) (2017) p. 8.

[137] R. Sparks, B. N. Bloch, E. Feleppa *et al.*, Fully automated prostate magnetic resonance imaging and transrectal ultrasound fusion via a probabilistic registration metric, *Medical Imaging 2013: Image-Guided Procedures, Robotic Interventions, and Modeling*, **8671**, SPIE (2013), pp. 72–85.

[138] O. Zettinig, A. Shah, C. Hennersperger *et al.*, Multimodal image-guided prostate fusion biopsy based on automatic deformable registration, *International Journal of Computer Assisted Radiology and Surgery* **10**(12) (2015) 1997–2007.

[139] C. Weon, W. Hyun Nam, D. Lee *et al.*, Position tracking of moving liver lesion based on real-time registration between 2D ultrasound and 3D preoperative images, *Medical Physics* **42**(1) (2015) 335–347.

[140] A. Leroy, P. Mozer, Y. Payan *et al.*, Rigid registration of freehand 3D ultrasound and CT-scan kidney images, *International Conference on Medical Image Computing and Computer-Assisted Intervention*, Springer (2004), pp. 837–844.

[141] J. Gomes-Fonseca, S. Queirós, P. Morais *et al.*, Surface-based registration between CT and US for image-guided percutaneous renal access–A feasibility study, *Medical Physics* **46**(3) (2019) 1115–1126.

[142] H.-E. Gueziri, D. L. Collins, Fast registration of CT with intra-operative ultrasound images for spine surgery, *International Workshop and Challenge on Computational Methods and Clinical Applications for Spine Imaging*, Springer (2018), pp. 29–40.

[143] A. Chan, B. Coutts, E. Parent *et al.*, Development and evaluation of CT-to-3D ultrasound image registration algorithm in vertebral phantoms for spine surgery, *Annals of Biomedical Engineering* **49**(1) (2021) 310–321.

[144] H. Guo, H. Chao, S. Xu *et al.*, Ultrasound volume reconstruction from freehand scans without tracking, *IEEE Transactions on Biomedical Engineering* **70**(3) (2022) 970–979.

[145] G. Haskins, U. Kruger, P. Yan, Deep learning in medical image registration: A survey, *Machine Vision and Applications* **31**(1) (2020) p. 8.

[146] G. Haskins, J. Kruecker, U. Kruger *et al.*, Learning deep similarity metric for 3D MR–TRUS image registration, *International Journal of Computer Assisted Radiology and Surgery* **14**(3) (2019) 417–425.

[147] M. Yang, Q. Wang, S. Huang *et al.*, Det-SAMReg: Few-shot medical image registration using vision foundation models, *International Workshop on Advances in Simplifying Medical Ultrasound*, Springer (2025), pp. 76–86.

[148] X. Song, X. Xu, J. Zhang *et al.*, DINO-Reg: Efficient multimodal image registration with distilled features, *IEEE Transactions on Medical Imaging* **44**(9) (2025) 3809–3819.

[149] T. Ghosh, F. Sheikhi, J. Guo *et al.*, Foundation models for volumetric medical imaging: Opportunities, challenges, and future directions, *Electronics* **15**(6) (2026) p. 1245.

[150] M. Guo, X. Cheng, W. Lu *et al.*, Foundation-guided representation alignment for multimodal medical image registration, *European Conference on Computer Vision*, Springer (2026), pp. 518–535.

[151] X. Ma, X. Zhang, Y. Wang *et al.*, Cross-modality registration using bone surface pointcloud for robotic ultrasound-guided spine surgery, *Journal of medical robotics research* **10**(01n02) (2025) p. 2540004.

[152] E. Ferrante, N. Paragios, Slice-to-volume medical image registration: A survey, *Medical Image Analysis* **39** (2017) 101–123.

[153] R. Brooks, D. L. Collins, X. Morandi *et al.*, Deformable ultrasound registration without reconstruction, *International Conference on Medical Image Computing and Computer-Assisted Intervention*, Springer (2008), pp. 1023–1031.

[154] C. Peng, Q. Cai, M. Chen *et al.*, Recent advances in tracking devices for biomedical ultrasound imaging applications, *Micromachines* **13**(11) (2022) p. 1855.

[155] C. A. Adriaans, M. Wijkhuizen, L. M. van Karnenbeek *et al.*, Trackerless 3D freehand ultrasound reconstruction: A review, *Applied Sciences* **14**(17) (2024) p. 7991.

[156] Y. Lu, K. Fan, J. Yuan *et al.*, Free scan real time 3D ultrasound imaging with shading artefacts removal, *Ultrasonics* **135** (2023) p. 107091.

[157] C.-H. Lin, Y.-N. Sun, C.-J. Lin, A motion compounding technique for speckle reduction in ultrasound images, *Journal of Digital Imaging* **23**(3) (2010) 246–257.

[158] Q. Zou, Y. Huang, J. Gao *et al.*, Three-dimensional ultrasound image reconstruction based on 3D-ResNet in the musculoskeletal system using a 1D probe: ex vivo and in vivo feasibility studies, *Physics in Medicine and Biology* **68**(16) (2023) p. 165003.

[159] C. Victoria, F. Torres, E. Garduño *et al.*, Real-time 3D ultrasound reconstruction using octrees, *IEEE Access* **11** (2023) 78970–78983.

[160] R. Rohling, A. Gee, L. Berman, Three-dimensional spatial compounding of ultrasound images, *Medical Image Analysis* **1**(3) (1997) 177–193.

[161] D. F. Leotta, R. W. Martin, Three-dimensional spa-

tial compounding of ultrasound scans with weighting by incidence angle, *Ultrasonic Imaging* **22**(1) (2000) 1–19.

[162] V. Grau, J. A. Noble, Adaptive multiscale ultrasound compounding using phase information, *International Conference on Medical Image Computing and Computer-Assisted Intervention*, Springer (2005), pp. 589–596.

[163] C. Yao, J. M. Simpson, T. Schaeffter *et al.*, Multi-view 3D echocardiography compounding based on feature consistency, *Physics in Medicine and Biology* **56**(18) (2011) p. 6109.

[164] J. Perez-Gonzalez, F. Arámbula-Cosío, M. Guzmán *et al.*, Spatial compounding of 3-D fetal brain ultrasound using probabilistic maps, *Ultrasound in Medicine & Biology* **44**(1) (2018) 278–291.

[165] J. Perez-Gonzalez, N. Hevia Montiel, V. M. Bañuelos, Deep learning spatial compounding from multiple fetal head ultrasound acquisitions, *International Workshop on Advances in Simplifying Medical Ultrasound*, Springer (2020), pp. 305–314.

[166] R. Wright, A. Gomez, V. A. Zimmer *et al.*, Fast fetal head compounding from multi-view 3D ultrasound, *Medical Image Analysis* **89** (2023) p. 102793.

[167] C. S. z. Berge, A. Kapoor, N. Navab, Orientation-driven ultrasound compounding using uncertainty information, *Information Processing in Computer-Assisted Interventions*, eds.D. Stoyanov, D. L. Collins, I. Sakuma *et al.* (Springer International Publishing, Cham, 2014), pp. 236–245.

[168] H. Mazdarani, R. Hibbert, J. Watterson *et al.*, Confidence-aware 3D spatial compounding of 2D ultrasound images for needle shadow removal, *2025 IEEE Sensors Applications Symposium (SAS)*, IEEE (2025), pp. 1–6.

[169] F. Mohamed, C. V. Siang, A survey on 3D ultrasound reconstruction techniques, *Artificial Intelligence—Applications in Medicine and Biology* (2019) 73–92.

[170] X. Chen, H. Chen, Y. Peng *et al.*, A freehand 3D ultrasound reconstruction method based on deep learning, *Electronics* **12**(7) (2023) p. 1527.

[171] T. K. Chen, A. D. Thurston, M. H. Moghari *et al.*, A real-time ultrasound calibration system with automatic accuracy control and incorporation of ultrasound section thickness, *Medical Imaging 2008: Visualization, Image-Guided Procedures, and Modeling*, **6918**, SPIE (2008), pp. 766–776.

[172] S.-W. Chung, C.-C. Shih, C.-C. Huang, Freehand three-dimensional ultrasound imaging of carotid artery using motion tracking technology, *Ultrasonics* **74** (2017) 11–20.

[173] Z. Jiang, N. Danis, Y. Bi *et al.*, Precise repositioning of robotic ultrasound: Improving registration-based motion compensation using ultrasound confidence optimization, *IEEE Transactions on Instrumentation and Measurement* **71** (2022) 1–11.

[174] L. A. Groves, B. VanBerlo, N. Veinberg *et al.*, Automatic segmentation of the carotid artery and internal jugular vein from 2D ultrasound images for 3D vascular reconstruction, *International Journal of Computer Assisted Radiology and Surgery* **15**(11) (2020) 1835–1846.

[175] A. Fenster, G. Parraga, J. Bax, Three-dimensional ultrasound scanning, *Interface Focus* **1**(4) (2011) 503–519.

[176] M. I. Daoud, A.-L. Alshalalfah, F. Awwad *et al.*, Freehand 3D ultrasound imaging system using electromagnetic tracking, *2015 International Conference on Open Source Software Computing (OSSCOM)*, IEEE (2015), pp. 1–5.

[177] W. Jiang, X. Chen, C. Yu, A real-time freehand 3D ultrasound imaging method for scoliosis assessment, *Journal of Applied Clinical Medical Physics* **23**(8) (2022) p. e13709.

[178] Z. Chen, Q. Huang, Real-time freehand 3D ultrasound imaging, *Computer Methods in Biomechanics and Biomedical Engineering: Imaging & Visualization* **6**(1) (2018) 74–83.

[179] M. Wijkhuizen, C. A. Adriaans, L. M. van Karnenbeek *et al.*, 3D ultrasound volume reconstruction using a CNN-transformer model and IMU data, *International Workshop on Advances in Simplifying Medical Ultrasound*, Springer (2025), pp. 43–52.

[180] T. Kim, D.-H. Kang, S. Shim *et al.*, Versatile low-cost volumetric 3D ultrasound imaging using gimbal-assisted distance sensors and an inertial measurement unit, *Sensors* **20**(22) (2020) p. 6613.

[181] R. Prevost, M. Salehi, S. Jagoda *et al.*, Deep learning-based 3D freehand ultrasound reconstruction with inertial measurement units, *Medical Image Analysis* (2018).

[182] R. Li, A. Davoodi, Y. Cai *et al.*, Robot-assisted ultrasound reconstruction for spine surgery: From bench-top to pre-clinical study, *International Journal of Computer Assisted Radiology and Surgery* **18**(9) (2023) 1613–1623.

[183] M. Ding, A. Fenster, A real-time biopsy needle segmentation technique using hough transform, *Medical Physics* **30**(8) (2003) 2222–2233.

[184] W. Qiu, H. Zhou, M. Ding *et al.*, New real time needle segmentation technique using grayscale hough transformation, *MIPPR 2007: Medical Imaging, Parallel Processing of Images, and Optimization Techniques*, **6789**, SPIE (2007), pp. 183–190.

[185] E. Ayvali, J. P. Desai, Optical flow-based tracking of needles and needle-tip localization using circular hough transform in ultrasound images, *Annals of Biomedical Engineering* **43**(8) (2015) 1828–1840.

[186] W. Yan, Q. Ding, J. Chen *et al.*, Needle tip tracking in 2D ultrasound based on improved compressive tracking and adaptive kalman filter, *IEEE Robotics and Automation Letters* **6**(2) (2021) 3224–3231.

[187] S. Hans, P. Bansal, G. Mathur *et al.*, Experimental evaluation of needle tip prediction using kalman filtering approach, *International Conference on Com-*

puter Vision and Image Processing, Springer (2023), pp. 283–292.

[188] M. Aboofazeli, P. Abolmaesumi, P. Mousavi *et al.*, A new scheme for curved needle segmentation in three-dimensional ultrasound images, *2009 IEEE International Symposium on Biomedical Imaging: From Nano to Macro*, IEEE (2009), pp. 1067–1070.

[189] C. Nadeau, A. Krupa, J. Petr *et al.*, Moments-based ultrasound visual servoing: From a mono-to multiplane approach, *IEEE Transactions on Robotics* **32**(6) (2016) 1558–1564.

[190] S. Grube, S. Latus, F. Behrendt *et al.*, Needle tracking in low-resolution ultrasound volumes using deep learning, *International Journal of Computer Assisted Radiology and Surgery* **19**(10) (2024) 1975–1981.

[191] W. Yan, Q. Ding, J. Chen *et al.*, Learning-based needle tip tracking in 2D ultrasound by fusing visual tracking and motion prediction, *Medical Image Analysis* **88** (2023) p. 102847.

[192] Q. Zhang, J. Chen, J. Wang *et al.*, Needle tracking and segmentation in breast ultrasound imaging based on spatio-temporal memory network, *Frontiers in Oncology* **14** (2025) p. 1519536.

[193] A. M. Wijata, B. Pyciński, J. Nalepa, A needle in a (medical) haystack: Detecting a biopsy needle in ultrasound images using vision transformers, *2024 IEEE International Conference on Image Processing (ICIP)*, (2024), pp. 3017–3023.

[194] A. Ranne, L. Kuang, Y. Velikova *et al.*, CathFlow: Self-supervised segmentation of catheters in interventional ultrasound using optical flow and transformers, *2024 IEEE/RSJ International Conference on Intelligent Robots and Systems (IROS)*, (2024), pp. 2436–2443.

[195] D. Huang, C. Li, A. Karlas *et al.*, VibNet: Vibration-boosted needle detection in ultrasound images, *IEEE Transactions on Medical Imaging* **44**(6) (2025) 2696–2708.

[196] S. M. Klein, M. P. Fronheiser, J. Reach *et al.*, Piezoelectric vibrating needle and catheter for enhancing ultrasound-guided peripheral nerve blocks, *Anesthesia & Analgesia* **105**(6) (2007) 1858–1860.

[197] Z. Shen, Y. Zhou, J. Miao *et al.*, Enhanced visualization of fine needles under sonographic guidance using a MEMS actuator, *Sensors* **15**(2) (2015) 3107–3115.

[198] Y. Kuang, A. Hilgers, M. Sadiq *et al.*, Modelling and characterisation of a ultrasound-actuated needle for improved visibility in ultrasound-guided regional anaesthesia and tissue biopsy, *Ultrasonics* **69** (2016) 38–46.

[199] C. Baker, M. Xochicale, F.-Y. Lin *et al.*, Intraoperative needle tip tracking with an integrated fibre-optic ultrasound sensor, *Sensors* **22**(23) (2022) p. 9035.

[200] H. J. Kang, X. Guo, A. Cheng *et al.*, Needle visualization using photoacoustic effect, *Photons plus ultrasound: imaging and sensing 2015*, **9323**, SPIE (2015), pp. 441–447.

[201] W. Xia, J. M. Mari, S. J. West *et al.*, In-plane ultrasonic needle tracking using a fiber-optic hydrophone, *Medical Physics* **42**(10) (2015) 5983–5991.

[202] H. Lu, J. Li, Q. Lu *et al.*, A new sensor technology for 2D ultrasound-guided needle tracking, *International Conference on Medical Image Computing and Computer-Assisted Intervention*, Springer (2014), pp. 389–396.

[203] A. Hakime, A. Barah, F. Deschamps *et al.*, Prospective comparison of freehand and electromagnetic needle tracking for us-guided percutaneous liver biopsy, *Journal of Vascular and Interventional Radiology* **24**(11) (2013) 1682–1689.

[204] E. B. Levy, J. Tang, D. Lindisch *et al.*, Implementation of an electromagnetic tracking system for accurate intrahepatic puncture needle guidance: Accuracy results in an in vitro model, *Academic Radiology* **14**(3) (2007) 344–354.

[205] J. Krücker, S. Xu, N. Glossop *et al.*, Electromagnetic tracking for thermal ablation and biopsy guidance: Clinical evaluation of spatial accuracy, *Journal of Vascular and Interventional Radiology* **18**(9) (2007) 1141–1150.

[206] K. Mathiassen, D. Dall'Alba, R. Muradore *et al.*, Real-time biopsy needle tip estimation in 2D ultrasound images, *2013 IEEE International Conference on Robotics and Automation*, IEEE (2013), pp. 4363–4369.

[207] P. J. Stolka, P. Foroughi, M. Rendina *et al.*, Needle guidance using handheld stereo vision and projection for ultrasound-based interventions, *International Conference on Medical Image Computing and Computer-Assisted Intervention*, Springer (2014), pp. 684–691.

[208] H. Che, J. Qin, Y. Chen *et al.*, Improving needle tip tracking and detection in ultrasound-based navigation system using deep learning-enabled approach, *IEEE Journal of Biomedical and Health Informatics* **28**(5) (2024) 2930–2942.

[209] W. He, R. L. Qiu, C. Zhang *et al.*, Trackerless 3D ultrasound volume reconstruction from 2d freehand scans using a hybrid transformer–CNN framework, *Medical Physics* **52**(11) (2025) p. e70103.

[210] C. Rossa, M. Tavakoli, Issues in closed-loop needle steering, *Control Engineering Practice* **62** (2017) 55–69.

[211] H. Yang, C. Shan, A. F. Kolen *et al.*, Medical instrument detection in ultrasound: A review, *Artificial Intelligence Review* **56**(5) (2023) 4363–4402.

[212] G. McLeod, Novel approaches to needle tracking and visualisation, *Anaesthesia* **76** (2021) 160–170.

[213] Z. Zhao, Z. T. H. Tse, An electromagnetic tracking needle clip: An enabling design for low-cost image-guided therapy, *Minimally Invasive Therapy & Allied Technologies* **28**(3) (2019) 165–171.

[214] B. J. Wood, H. Zhang, A. Durrani *et al.*, Navigation with electromagnetic tracking for interventional radiology procedures: A feasibility study, *Journal of Vascular and Interventional Radiology* **16**(4) (2005)

493–505.

[215] P. Chatelain, A. Krupa, M. Marchal, Real-time needle detection and tracking using a visually servoed 3D ultrasound probe, *2013 IEEE International Conference on Robotics and Automation*, IEEE (2013), pp. 1676–1681.

[216] P. Beigi, P. Malenfant, A. Rasoulian *et al.*, Three-dimensional ultrasound-guided real-time midline epidural needle placement with epiguide: A prospective feasibility study, *Ultrasound in Medicine & Biology* **43**(1) (2017) 375–379.

[217] C. Nadeau, A. Krupa, Intensity-based ultrasound visual servoing: Modeling and validation with 2D and 3D probes, *IEEE Transactions on Robotics* **29**(4) (2013) p. 1003.

[218] Z. Cheng, S. L. B. Sørensen, M. W. Olsen *et al.*, Needle tip tracking based on optical imaging and AI, *IEEE Sensors Journal* **24**(17) (2024) 28145–28153.

[219] J. Lazarus, M. Asselin, L. Kaestner, Optically tracked needle for ultrasound-guided percutaneous nephrolithotomy puncture: A preliminary report, *Journal of Endourology* **35**(12) (2021) 1733–1737.

[220] A. N. Johnson, J. S. Peiffer, N. Halmann *et al.*, Ultrasound-guided needle technique accuracy: Prospective comparison of passive magnetic tracking versus unassisted echogenic needle localization, *Regional Anesthesia & Pain Medicine* **42**(2) (2017) 223–232.

[221] K. März, A. M. Franz, A. Seitel *et al.*, Interventional real-time ultrasound imaging with an integrated electromagnetic field generator, *International Journal of Computer Assisted Radiology and Surgery* **9**(5) (2014) 759–768.

[222] W. Liu, Z. Yang, P. Fang *et al.*, Deflection simulation for a needle adjusted by the insertion orientation angle and axial rotation during insertion in the muscle-contained double-layered tissue, *Medical & Biological Engineering & Computing* **58**(10) (2020) 2291–2304.

[223] C. Jun, S. Lim, D. Petrisor *et al.*, A simple insertion technique to reduce the bending of thinbevel-point needles, *Minimally Invasive Therapy & Allied Technologies* **28**(4) (2019) 199–205.

[224] C. Rossa, M. Khadem, R. Sloboda *et al.*, Adaptive quasi-static modelling of needle deflection during steering in soft tissue, *IEEE Robotics and Automation Letters* **1**(2) (2016) 916–923.

[225] B. Zhao, L. Lei, L. Xu *et al.*, Needle deflection modeling and preoperative trajectory planning during insertion into multilayered tissues, *IEEE/ASME Transactions on Mechatronics* **26**(2) (2020) 943–954.

[226] B. Konh, B. Padasdao, Z. Batsaikhan *et al.*, Integrating robot-assisted ultrasound tracking and 3D needle shape prediction for real-time tracking of the needle tip in needle steering procedures, *The International Journal of Medical Robotics and Computer Assisted Surgery* **17**(4) (2021) p. e2272.

[227] H. Sadjadi, K. Hashtrudi-Zaad, G. Fichtinger, Fusion of electromagnetic trackers to improve needle deflection estimation: Simulation study, *IEEE Transactions on Biomedical Engineering* **60**(10) (2013) 2706–2715.

[228] R. P. Pal, A. J. Koupparis, Expanding the indications of robotic surgery in urology: A systematic review of the literature, *Arab Journal of Urology* **16**(3) (2018) 270–284.

[229] K. Taguchi, S. Hamamoto, A. Okada *et al.*, A randomized, single-blind clinical trial comparing robotic-assisted fluoroscopic-guided with ultrasound-guided renal access for percutaneous nephrolithotomy, *The Journal of Urology* **208**(3) (2022) 684–694.

[230] F. J. Siepel, B. Maris, M. K. Welleweerd *et al.*, Needle and biopsy robots: A review, *Current Robotics Reports* **2**(1) (2021) 73–84.

[231] Z. Jiang, S. E. Salcudean, N. Navab, Robotic ultrasound imaging: State-of-the-art and future perspectives, *Medical Image Analysis* **89** (2023) p. 102878.

[232] C. Kim, D. Chang, D. Petrisor *et al.*, Ultrasound probe and needle-guide calibration for robotic ultrasound scanning and needle targeting, *IEEE Transactions on Biomedical Engineering* **60**(6) (2013) 1728–1734.

[233] R. K. Gupta, J. Lane, B. Allen *et al.*, Improving needle visualization by novice residents during an in-plane ultrasound nerve block simulation using an in-plane multiangle needle guide, *Pain Medicine* **14**(10) (2013) 1600–1607.

[234] H. Ueshima, A. Kitamura, The use of a needle guide kit improves the stability of ultrasound-guided techniques, *Journal of Anesthesia* **29**(5) (2015) 803–804.

[235] T. Cho, N. Komasawa, M. Haba *et al.*, Needle guides for venous catheter insertion during chest compressions: a crossover simulation trial, *The American Journal of Emergency Medicine* **34**(6) (2016) 989–992.

[236] D. Stoianovici, C. Jun, S. Lim *et al.*, Multi-imager compatible, MR safe, remote center of motion needle-guide robot, *IEEE Transactions on Biomedical Engineering* **65**(1) (2017) 165–177.

[237] S. Chen, F. Wang, Y. Lin *et al.*, Ultrasound-guided needle insertion robotic system for percutaneous puncture, *International Journal of Computer Assisted Radiology and Surgery* **16**(3) (2021) 475–484.

[238] H. Li, T. He, M. Yang *et al.*, An ultrasound-guided miniature hand-eye integrated robot for percutaneous needle placement, *Journal of Mechanisms and Robotics* **17**(6) (2025) p. 065001.

[239] M. Kaya, E. Senel, A. Ahmad *et al.*, Visual needle tip tracking in 2D US guided robotic interventions, *Mechatronics* **57** (2019) 129–139.

[240] O. Wilz, B. Kent, B. Sainsbury *et al.*, Multiobjective trajectory tracking of a flexible tool during robotic percutaneous nephrolithotomy, *IEEE Robotics and Automation Letters* **6**(4) (2021) 8110–8117.

[241] G. Zheng, X. Zhao, T. Chen *et al.*, A simultaneous ultrasound-robot calibration approach for dual-robot intervention by solving the AXP= YCQ problem,

IEEE Transactions on Instrumentation and Measurement **73** (2024) 1–10.

[242] W. Zhang, S. Wang, L. Xie *et al.*, An autonomous liver biopsy robotic system under respiratory motion, *IEEE Transactions on Instrumentation and Measurement* **74** (2025) 1–10.

[243] T. K. Adebar, A. E. Fletcher, A. M. Okamura, 3-D ultrasound-guided robotic needle steering in biological tissue, *IEEE Transactions on Biomedical Engineering* **61**(12) (2014) 2899–2910.

[244] C. Rossa, N. Usmani, R. Sloboda *et al.*, A handheld assistant for semiautomated percutaneous needle steering, *IEEE Transactions on Biomedical Engineering* **64**(3) (2016) 637–648.

[245] B. Fallahi, C. Rossa, R. S. Sloboda *et al.*, Slidingbased image-guided 3D needle steering in soft tissue, *Control Engineering Practice* **63** (2017) 34–43.

[246] D. Beiko *et al.*, Techniques–ultrasound-guided percutaneous nephrolithotomy: How we do it, *Canadian Urological Association Journal* **14**(3) (2020) p. E104.

[247] I. Boekestijn, S. Azargoshasb, M. N. van Oosterom *et al.*, Value-assessment of computer-assisted navigation strategies during percutaneous needle placement, *International Journal of Computer Assisted Radiology and Surgery* **17**(10) (2022) 1775–1785.

[248] B. Fallahi, C. Rossa, R. S. Sloboda *et al.*, Slidingbased switching control for image-guided needle steering in soft tissue, *IEEE Robotics and Automation Letters* **1**(2) (2016) 860–867.

[249] T. L. De Jong, N. J. Van De Berg, L. Tas *et al.*, Needle placement errors: Do we need steerable needles in interventional radiology?, *Medical Devices: Evidence and Research* (2018) 259–265.

[250] F. Aalamifar, R. Khurana, A. Cheng *et al.*, Enabling technologies for robot assisted ultrasound tomography, *The International Journal of Medical Robotics and Computer Assisted Surgery* **13**(1) (2017) p. e1746.

[251] Y. Bi, Z. Jiang, F. Duelmer *et al.*, Machine learning in robotic ultrasound imaging: Challenges and perspectives, *Annual Review of Control, Robotics, and Autonomous Systems* **7** (2024).

[252] Q. Huang, J. Zhou, Z. Li, Review of robot-assisted medical ultrasound imaging systems: Technology and clinical applications, *Neurocomputing* **559** (2023) p. 126790.

[253] K. Li, Y. Xu, M. Q.-H. Meng, An overview of systems and techniques for autonomous robotic ultrasound acquisitions, *IEEE Transactions on Medical Robotics and Bionics* **3**(2) (2021) 510–524.

[254] S. E. Salcudean, H. Moradi, D. G. Black *et al.*, Robot-assisted medical imaging: A review, *Proceedings of the IEEE* **110**(7) (2022) 951–967.

[255] F. Von Haxthausen, S. Böttger, D. Wulff *et al.*, Medical robotics for ultrasound imaging: Current systems and future trends, *Current Robotics Reports* **2**(1) (2021) 55–71.

[256] R. Nakadate, J. Solis, A. Takanishi *et al.*, Implementation of an automatic scanning and detection algorithm for the carotid artery by an assisted-robotic measurement system, *2010 IEEE/RSJ International Conference on Intelligent Robots and Systems*, IEEE (2010), pp. 313–318.

[257] A. S. B. Mustafa, T. Ishii, Y. Matsunaga *et al.*, Development of robotic system for autonomous liver screening using ultrasound scanning device, *2013 IEEE international conference on robotics and biomimetics (ROBIO)*, IEEE (2013), pp. 804–809.

[258] C. Pahl, E. Supriyanto, Design of automatic transabdominal ultrasound imaging system, *2015 20th International Conference on Methods and Models in Automation and Robotics (MMAR)*, IEEE (2015), pp. 435–440.

[259] R. Tsumura, H. Iwata, Robotic fetal ultrasonography platform with a passive scan mechanism, *International Journal of Computer Assisted Radiology and Surgery* **15**(8) (2020) 1323–1333.

[260] M. K. Welleweerd, A. G. de Groot, S. De Looijer *et al.*, Automated robotic breast ultrasound acquisition using ultrasound feedback, *2020 IEEE International Conference on Robotics and Automation (ICRA)*, IEEE (2020), pp. 9946–9952.

[261] J. T. Kaminski, K. Rafatzand, H. K. Zhang, Feasibility of robot-assisted ultrasound imaging with force feedback for assessment of thyroid diseases, *Proceedings of SPIE–the International Society for Optical Engineering*, **11315** (2020), p. 113151D.

[262] Q. Huang, J. Lan, X. Li, Robotic arm based automatic ultrasound scanning for three-dimensional imaging, *IEEE Transactions on Industrial Informatics* **15**(2) (2018) 1173–1182.

[263] R. Kojcev, A. Khakzar, B. Fuerst *et al.*, On the reproducibility of expert-operated and robotic ultrasound acquisitions, *International Journal of Computer Assisted Radiology and Surgery* **12**(6) (2017) 1003–1011.

[264] C. Hennersperger, B. Fuerst, S. Virga *et al.*, Towards MRI-based autonomous robotic us acquisitions: A first feasibility study, *IEEE Transactions on Medical Imaging* **36**(2) (2016) 538–548.

[265] S. Merouche, L. Allard, E. Montagnon *et al.*, A robotic ultrasound scanner for automatic vessel tracking and three-dimensional reconstruction of B-mode images, *IEEE Transactions on Ultrasonics, Ferroelectrics, and Frequency Control* **63**(1) (2015) 35–46.

[266] J. Housden, S. Wang, X. Bao *et al.*, Towards standardized acquisition with a dual-probe ultrasound robot for fetal imaging, *IEEE Robotics and Automation Letters* **6**(2) (2021) 1059–1065.

[267] H. Mazdarani, B. Sainsbury, J. Watterson *et al.*, Ultrasound-based visual servoing for out-of-plane longitudinal needle tracking in robot-aided percutaneous nephrolithotomy, *IEEE Access* **13** (2025) 69090–69102.

[268] Y. J. Kim, J. H. Seo, H. R. Kim *et al.*, Development of a control algorithm for the ultrasound scan-

ning robot (NCCUSR) using ultrasound image and force feedback, *The International Journal of Medical Robotics and Computer Assisted Surgery* **13**(2) (2017) p. e1756.

[269] F. Suligoj, C. M. Heunis, J. Sikorski *et al.*, Robust–an autonomous robotic ultrasound system for medical imaging, *IEEE Access* **9** (2021) 67456–67465.

[270] Z. Jiang, M. Grimm, M. Zhou *et al.*, Automatic normal positioning of robotic ultrasound probe based only on confidence map optimization and force measurement, *IEEE Robotics and Automation Letters* **5**(2) (2020) 1342–1349.

[271] J. Jiang, J. Luo, H. Wang *et al.*, Force tracking control method for robotic ultrasound scanning system under soft uncertain environment, *Actuators*, **13**(2), MDPI (2024), p. 62.

[272] M. W. Gilbertson, B. W. Anthony, Force and position control system for freehand ultrasound, *IEEE Transactions on Robotics* **31**(4) (2015) 835–849.

[273] R. Finocchi, F. Aalamifar, T. Y. Fang *et al.*, Co-robotic ultrasound imaging: A cooperative force control approach, *Medical Imaging 2017: Image-Guided Procedures, Robotic Interventions, and Modeling*, **10135**, (SPIE, 2017), pp. 270–280.

[274] T.-Y. Fang, H. K. Zhang, R. Finocchi *et al.*, Force-assisted ultrasound imaging system through dual force sensing and admittance robot control, *International Journal of Computer Assisted Radiology and Surgery* **12**(6) (2017) 983–991.

[275] J. Tan, B. Li, Y. Leng *et al.*, Fully automatic dual-probe lung ultrasound scanning robot for screening triage, *IEEE Transactions on Ultrasonics, Ferroelectrics, and Frequency Control* **70**(9) (2022) 975–988.

[276] X. Ma, Z. Zhang, H. K. Zhang, Autonomous scanning target localization for robotic lung ultrasound imaging, *2021 IEEE/RSJ International Conference on Intelligent Robots and Systems (IROS)*, IEEE (2021), pp. 9467–9474.

[277] S. Virga, O. Zettinig, M. Esposito *et al.*, Automatic force-compliant robotic ultrasound screening of abdominal aortic aneurysms, *2016 IEEE/RSJ international conference on intelligent robots and systems (IROS)*, IEEE (2016), pp. 508–513.

[278] S. Chen, Z. Li, Y. Lin *et al.*, Automatic ultrasound scanning robotic system with optical waveguide-based force measurement, *International Journal of Computer Assisted Radiology and Surgery* **16**(6) (2021) 1015–1025.

[279] G. Ning, J. Chen, X. Zhang *et al.*, Force-guided autonomous robotic ultrasound scanning control method for soft uncertain environment, *International Journal of Computer Assisted Radiology and Surgery* **16**(12) (2021) 2189–2199.

[280] J. Wang, C. Lu, Y. Lv *et al.*, Task space compliant control and six-dimensional force regulation toward automated robotic ultrasound imaging, *IEEE Transactions on Automation Science and Engineering* **21**(3) (2023) 3652–3663.

[281] P. Chatelain, A. Krupa, N. Navab, Optimization of ultrasound image quality via visual servoing, *2015 IEEE International Conference on Robotics and Automation (ICRA)*, (IEEE, Seattle, WA, USA, 2015), pp. 5997–6002.

[282] F. Abhimanyu, Improving robotic ultrasound AI using optical flow, Master's thesis, Carnegie Mellon University (2023).

[283] D. Dall'Alba, L. Busellato, T. R. Savarimuthu *et al.*, Imitation learning of compression pattern in robotic assisted ultrasound examination using kernelized movement primitives, *IEEE Transactions on Medical Robotics and Bionics* **6**(4) (2024) 1567–1580.

[284] S. Zhang, B. Ouyang, C. Zhao *et al.*, Ultra-malin: Robotic ultrasound mapping and localization via implicit neural representation, *IEEE Transactions on Instrumentation and Measurement* **74** (2025) 1–12.

[285] M. Afshar, J. Carriere, T. Meyer *et al.*, Autonomous ultrasound scanning to localize needle tip in breast brachytherapy, *2020 International Symposium on Medical Robotics (ISMR)*, IEEE (2020), pp. 202–208.

[286] J. Lee, B. Lala, S. Y. Ko, Three-dimensional needle shape reconstruction using robotic ultrasound tracking system with U-Net-based segmentation model, *International Journal of Control, Automation and Systems* **23**(8) (2025) 2420–2432.

[287] F. Aalamifar, R. Khurana, A. Cheng *et al.*, Enabling technologies for robot assisted ultrasound tomography: system setup and calibration, *Medical Imaging 2014: Ultrasonic Imaging and Tomography*, **9040**, SPIE (2014), pp. 495–503.

[288] H. Yang, D. Yang, L. Zhang *et al.*, Robot-assisted automatic ultrasound calibration without external trackers, *IEEE Transactions on Instrumentation and Measurement* **74** (2025) 1–10.

[289] F. Chaumette, S. Hutchinson, Visual servo control. I. basic approaches, *IEEE Robotics & Automation Magazine* **13**(4) (2006) 82–90.

[290] M. L. Balter, A. I. Chen, T. J. Maguire *et al.*, Adaptive kinematic control of a robotic venipuncture device based on stereo vision, ultrasound, and force guidance, *IEEE Transactions on Industrial Electronics* **64**(2) (2016) 1626–1635.

[291] S. M. Sajadi, S. M. Karbasi, H. Brun *et al.*, Towards autonomous robotic biopsy—design, modeling and control of a robot for needle insertion of a commercial full core biopsy instrument, *Frontiers in Robotics and AI* **9** (2022) p. 896267.

[292] Y. Lin, S. Chen, W. Xu *et al.*, Robotic system for accurate percutaneous puncture guided by 3D–2D ultrasound, *International Journal of Computer Assisted Radiology and Surgery* **18**(2) (2023) 217–225.

[293] J. Hong, T. Dohi, M. Hashizume *et al.*, An ultrasound-driven needle-insertion robot for percutaneous cholecystostomy, *Physics in Medicine and Biology* **49**(3) (2004) 441–455.

[294] F. von Haxthausen, T. Aust, H. Schwegmann

et al., Visual servoing for semi-automated 2D ultrasound scanning of peripheral arteries, *AUTOMED-Automation in Medical Engineering*, **1**(1) (2020).

[295] R. Mebarki, A. Krupa, F. Chaumette, 2-D ultrasound probe complete guidance by visual servoing using image moments, *IEEE Transactions on Robotics* **26**(2) (2010) 296–306.

[296] R. Kojcev, B. Fuerst, O. Zettinig *et al.*, Dual-robot ultrasound-guided needle placement: Closing the planning-imaging-action loop, *International Journal of Computer Assisted Radiology and Surgery* **11**(6) (2016) 1173–1181.

[297] J. Berger, M. Unger, J. Keller *et al.*, Design and validation of a medical robotic device system to control two collaborative robots for ultrasound-guided needle insertions, *Frontiers in Robotics and AI* **9** (2022) p. 875845.

[298] H. Mazdarani, J. Watterson, R. Hibbert *et al.*, Integrating confidence maps and visual servoing for needle tracking in robotic US-guided percutaneous nephrolithotomy, *IEEE Open Journal of Instrumentation and Measurement* (2025).

[299] O. Tahri, F. Chaumette, Point-based and region-based image moments for visual servoing of planar objects, *IEEE Transactions on Robotics* **21**(6) (2005) 1116–1127.

[300] R. Mebarki, A. Krupa, F. Chaumette, Image moments-based ultrasound visual servoing, *2008 IEEE International Conference on Robotics and Automation*, IEEE (2008), pp. 113–119.

[301] J. M. Romano, R. J. Webster, A. M. Okamura, Teleoperation of steerable needles, *Proceedings 2007 IEEE International Conference on Robotics and Automation*, IEEE (2007), pp. 934–939.

[302] R. V. Patel, S. F. Atashzar, M. Tavakoli, Haptic feedback and force-based teleoperation in surgical robotics, *Proceedings of the IEEE* **110**(7) (2022) 1012–1027.

[303] W. Si, N. Wang, C. Yang, Design and quantitative assessment of teleoperation-based human–robot collaboration method for robot-assisted sonography, *IEEE Transactions on Automation Science and Engineering* **22** (2024) 317–327.

[304] R. Ye, X. Zhou, F. Shao *et al.*, Feasibility of a 5G-based robot-assisted remote ultrasound system for cardiopulmonary assessment of patients with coronavirus disease 2019, *Chest* **159**(1) (2021) 270–281.

[305] Z. Jiang, Y. Bi, M. Zhou *et al.*, Intelligent robotic sonographer: Mutual information-based disentangled reward learning from few demonstrations, *The International Journal of Robotics Research* **43**(7) (2024) 981–1002.

[306] C. Lauretti, R. Morfino, F. Cocco *et al.*, A teleoperated control for robot-aided percutaneous surgery: An application to needle insertion in nephrolithotomy, *IEEE Robotics and Automation Letters* **10**(11) (2025) 11570–11577.

[307] M. Aggravi, D. A. Estima, A. Krupa *et al.*, Haptic teleoperation of flexible needles combining 3D ultrasound guidance and needle tip force feedback, *IEEE Robotics and Automation Letters* **6**(3) (2021) 4859–4866.

[308] A. C. Avila, M. Selim, M. Abayazid, Respiratory motion compensation and haptic feedback for X-ray-guided teleoperated robotic needle insertion, *2024 10th IEEE RAS/EMBS International Conference for Biomedical Robotics and Biomechatronics (BioRob)*, IEEE (2024), pp. 1352–1357.

[309] P. Baksic, H. Courtecuisse, B. Bayle, Shared control strategy for needle insertion into deformable tissue using inverse finite element simulation, *2021 IEEE International Conference on Robotics and Automation (ICRA)*, IEEE (2021), pp. 12442–12448.

[310] A. Ehrampoosh, B. Shirinzadeh, J. Pinskier *et al.*, A force-feedback methodology for teleoperated suturing task in robotic-assisted minimally invasive surgery, *Sensors* **22**(20) (2022) p. 7829.

[311] O. Gerovichev, P. Marayong, A. M. Okamura, The effect of visual and haptic feedback on manual and teleoperated needle insertion, *International Conference on Medical Image Computing and Computer-Assisted Intervention*, Springer (2002), pp. 147–154.

[312] C. Esposito, G. Autorino, M. Castagnetti *et al.*, Robotics and future technical developments in pediatric urology, *Seminars in Pediatric Surgery*, **30**(4), Elsevier (2021), p. 151082.

[313] C. Delgorge, F. Courrèges, L. A. Bassit *et al.*, A teleoperated mobile ultrasound scanner using a light-weight robot, *IEEE Transactions on Information Technology in Biomedicine* **9**(1) (2005) 50–58.

[314] J. Zhou, B. Gao, B. Xue *et al.*, Real-time interaction of a 7-DOF robot for teleoperated ultrasonic scanning, *2021 6th IEEE International Conference on Advanced Robotics and Mechatronics (ICARM)*, IEEE (2021), pp. 483–486.

[315] Q. Huang, J. Lan, Remote control of a robotic prosthesis arm with six-degree-of-freedom for ultrasonic scanning and three-dimensional imaging, *Biomedical Signal Processing and Control* **54** (2019) p. 101606.

[316] B. Duan, L. Xiong, X. Guan *et al.*, Tele-operated robotic ultrasound system for medical diagnosis, *Biomedical Signal Processing and Control* **70** (2021) p. 102900.

[317] F. Conti, J. Park, O. Khatib, Interface design and control strategies for a robot assisted ultrasonic examination system, *Experimental Robotics: The 12th International Symposium on Experimental Robotics*, Springer (2014), pp. 97–113.

[318] K. Masuda, E. Kimura, N. Tateishi *et al.*, Three dimensional motion mechanism of ultrasound probe and its application for tele-echography system, *2001 IEEE/RSJ International Conference on Intelligent Robots and Systems*, **2**, IEEE (2001), pp. 1112–1116.

[319] A. Vilchis, J. Troccaz, P. Cinquin *et al.*, A new robot architecture for tele-echography, *IEEE Transactions on Robotics and Automation* **19**(5) (2003) 922–926.

[320] N. Koizumi, S. Warisawa, M. Nagoshi *et al.*, Construction methodology for a remote ultrasound diagnostic system, *IEEE Transactions on Robotics* **25**(3) (2009) 522–538.

[321] C. Schneider, A. Baghani, R. Rohling *et al.*, Remote ultrasound palpation for robotic interventions using absolute elastography, *International Conference on Medical Image Computing and Computer-Assisted Intervention*, Springer (2012), pp. 42–49.

[322] Y. Deng, Y. Tang, B. Yang *et al.*, A review of bilateral teleoperation control strategies with soft environment, *2021 6th IEEE International Conference on Advanced Robotics and Mechatronics (ICARM)*, IEEE (2021), pp. 459–464.

[323] N. Yilmaz, B. Burkhart, A. Deguet *et al.*, Enhancing robotic telesurgery with sensorless haptic feedback, *International Journal of Computer Assisted Radiology and Surgery* **19**(6) (2024) 1147–1155.

[324] S. Avgousti, E. G. Christoforou, A. S. Panayides *et al.*, Medical telerobotic systems: Current status and future trends, *BioMedical Engineering OnLine* **15**(1) (2016) p. 96.

[325] X. Ma, W.-Y. Kuo, K. Yang *et al.*, A-see: Active-sensing end-effector enabled probe self-normal-positioning for robotic ultrasound imaging applications, *IEEE Robotics and Automation Letters* **7**(4) (2022) 12475–12482.

[326] J. Carriere, J. Fong, T. Meyer *et al.*, An admittance-controlled robotic assistant for semi-autonomous breast ultrasound scanning, *2019 international symposium on medical robotics (ISMR)*, IEEE (2019), pp. 1–7.

[327] H. T. Şen, A. Cheng, K. Ding *et al.*, Cooperative control with ultrasound guidance for radiation therapy, *Frontiers in Robotics and AI* **3** (2016) p. 49.

[328] H.-Y. Li, I. Paranawithana, L. Yang *et al.*, Stable and compliant motion of physical human–robot interaction coupled with a moving environment using variable admittance and adaptive control, *IEEE Robotics and Automation Letters* **3**(3) (2018) 2493–2500.

[329] A. Cherubini, D. Navarro-Alarcon, Sensor-based control for collaborative robots: Fundamentals, challenges, and opportunities, *Frontiers in Neurorobotics* **14** (2021) p. 576846.

[330] A. Gottardi, S. Tortora, E. Tosello *et al.*, Shared control in robot teleoperation with improved potential fields, *IEEE Transactions on Human-Machine Systems* **52**(3) (2022) 410–422.

[331] Y. Xie, J. Guo, Z. Deng *et al.*, Robot-assisted transesophageal ultrasound and the virtual admittance-based master-slave control method thereof, *IEEE/ASME Transactions on Mechatronics* **28**(5) (2023) 2505–2516.

[332] D. Black, Y. Oloumi Yazdi, A. H. Hadi Hosseinabadi *et al.*, Human teleoperation–a haptically enabled mixed reality system for teleultrasound, *Human–Computer Interaction* **39**(5-6) (2024) 529–552.

[333] R. Göbl, S. Virga, J. Rackerseder *et al.*, Acoustic window planning for ultrasound acquisition, *International Journal of Computer Assisted Radiology and Surgery* **12**(6) (2017) 993–1001.

[334] R. Tsumura, T. Tomioka, Y. Koseki *et al.*, Safe contact force generation for robotic thyroid ultrasound imaging, *IEEE Robotics and Automation Letters* **9**(2) (2024) 1700–1707.

[335] H. Mazdarani, C. Rossa, Teleoperated ultrasound imaging with confidence map-based visual servoing for acoustic coupling optimization, *2026 IEEE Canadian Conference on Electrical and Computer Engineering (CCECE)*, (2026), pp. 946–951.

[336] M. Akbari, J. Carriere, R. Sloboda *et al.*, Robot-assisted breast ultrasound scanning using geometrical analysis of the seroma and image segmentation, *2021 IEEE/RSJ International Conference on Intelligent Robots and Systems (IROS)*, IEEE (2021), pp. 3784–3791.

[337] J. Zhan, J. Cartucho, S. Giannarou, Autonomous tissue scanning under free-form motion for intraoperative tissue characterisation, *2020 IEEE International Conference on Robotics and Automation (ICRA)*, IEEE (2020), pp. 11147–11154.

[338] E. M. Hidalgo, L. Wright, M. Isaksson *et al.*, Current applications of robot-assisted ultrasound examination, *Cardiovascular Imaging* **16**(2) (2023) 239–247.

[339] T. Han, G. Ning, H. Liang *et al.*, Toward clinical applications of intelligent robotic ultrasound systems, *IEEE Reviews in Biomedical Engineering* **19** (2026) 227–247.

[340] S. Chapala, J. Gibson, P. Chinniah *et al.*, Robotic ultrasound imaging: A comprehensive review of historical evolution, current state-of-the-art, and future perspectives, *Journal of Ultrasound in Medicine* (2026).